Icarus 441 (2025) 116666

Contents lists available at ScienceDirect

Icarus

journal homepage: www.elsevier.com/locate/icarus

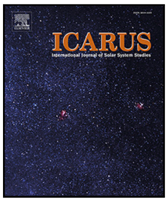

Research Paper

What is Mars (not) made of? A joint isotopic, geochemical and geophysical analysis

Christian Liebske [a,*], Amir Khan [a,c], Scott M. McLennan [a,b], Paolo A. Sossi [a]

[a] Institute of Geochemistry and Petrology, ETH Zürich, Switzerland
[b] Department of Geosciences, Stony Brook University, Stony Brook, NY, USA
[c] Institute of Geophysics, ETH Zürich, Switzerland

ARTICLE INFO

Keywords:
Mars
Nucleosynthetic isotopes
Chondrites
Major elements
Trace elements
Volatile elements
Bulk composition
Core
Geophysics
InSight

ABSTRACT

The terrestrial planets are believed to have accreted from chondritic meteorites of widely varying composition. Yet, making planets from known meteoritic material has proved elusive, be it their nucleosynthetic isotopic anomalies, bulk chemistry or geophysical properties. Because of the inherent non-uniqueness of meteoritic mixing models based on isotopes alone, combining geochemical and geophysical observations is key to identifying the nature of the building blocks of the terrestrial planets. Here, we integrate the recent proliferation of data in the form of geophysical measurements pertaining to Mars's interior structure from the recent InSight mission including its astronomic-geodetic response, the chemical and isotopic compositions of undifferentiated and differentiated meteorites, and observational constraints on trace element abundances (K/Th ratio) in order to make new inferences on the constitution and provenance of Mars. Using stochastic mixing models of meteoritic material, we find that ~0.02% of mixtures, consisting primarily of ordinary- and enstatite chondrites and, to a lesser extent, achondritic material, are able to reproduce the isotopic signature of Mars. Of these, however, none match the geophysical or Mg/Si and K/Th constraints, indicating that Mars is unlikely to have formed from known unmodified meteoritic material. Instead, relatively oxidised building blocks that are intrinsic to the inner solar system and underwent evaporation/condensation processes that lead to volatile-element depletion patterns unlike those in any known meteorite group, would be consistent with the isotopic, geochemical and geophysical properties of Mars.

1. Introduction

The compositions of undifferentiated meteorites, chondrites, owing to the constancy in their abundances of refractory elements, have been widely adopted as the building blocks of the terrestrial planets since the 1960s (e.g., Ringwood, 1966). These meteorites are sourced exclusively from parent bodies that reside(d) in the asteroid belt located at ~2.2–3.2 AU between Mars and Jupiter. The mass that currently resides in the belt collectively amounts to considerably less than 0.1% of the mass of the Earth. In addition to this shortfall of mass, forming the Earth and Mars from known meteoritic material (both chondritic and non-chondritic) has proved manifestly difficult, from the point of view of either bulk chemistry (e.g., Turekian and Clark, 1969; Drake and Righter, 2002; Righter et al., 2006; Campbell and O'Neill, 2012; Mezger et al., 2020; Sossi et al., 2022), isotopic anomalies (e.g., Lodders and Fegley, 1997; Sanloup et al., 1999; Mohapatra and Murty, 2003; Burbine and O'Brien, 2004; Tang and Dauphas, 2014; Fitoussi et al., 2016; Brasser et al., 2017; Dauphas et al., 2024) or geophysical properties that emerge from these compositions (e.g., Khan et al., 2018; Smrekar et al., 2019). However, like the parable of the blind men and the elephant (e.g. Saxe, 1873, p. 135–136), limited perspective inevitably leads to limited understanding.

Models that combine these three distinct, yet essential criteria for assessing whether mixtures of meteorites satisfy the constitution and structure of the planets are sparse. Other than the Earth, Mars is a prime target for such an analysis. Accordingly, Liebske and Khan (2019) combined isotopic anomalies in a range of meteorites to test whether mixtures thereof were consistent with the geophysical properties of Mars. These authors concluded that an oxidised, FeO-rich differentiated object (such as the angrite parent body), in addition to enstatite- and ordinary chondrite material, would be consistent with the internal structure of Mars determined at the time.

However, since 2019, the first direct seismic measurements of the basic internal structure of Mars were carried out as part of the InSight mission (e.g., Banerdt et al., 2020; Lognonné et al., 2023), revealing,

---

[*] Corresponding author.
E-mail address: christian.liebske@eaps.ethz.ch (C. Liebske).

https://doi.org/10.1016/j.icarus.2025.116666
Received 20 January 2025; Received in revised form 16 May 2025; Accepted 22 May 2025

among other features, a smaller, lower density core than previously thought (Khan et al., 2023; Samuel et al., 2023). This, in turn, furnishes powerful tests for physico-chemical models of accretion and compositional models in general (e.g., Khan et al., 2022). Numerous missions (including InSight) have produced high-quality astronomic-geodetic data that can be used to infer basic physical properties, such as mean density and moment of intertia (MoI) and tidal response (e.g., Konopliv et al., 2020; Le Maistre et al., 2023). It is also one of the few bodies (in addition to Mercury, Moon, 4-Vesta, 1-Ceres) for which there has been near planet-wide geochemical mapping of the surface by orbital gamma-ray spectroscopy, acting as a direct probe of its composition. Finally, nucleosynthetic isotopic anomalies, such as Mo and Zr in Martian meteorites measured in the last five years (e.g. Burkhardt et al., 2021; Render et al., 2022) permit tighter constraints to be placed on permissible combinations of meteoritic precursors.

Here, we aim to test the hypothesis that Mars is consistent with mixtures of known meteorites. We first review existing models that have attempted to reconstruct Mars from known meteorites mainly based on isotopic arguments. Next, we discuss additional major and minor element constraints, as well as the geophysical properties of Mars as seen by the recent InSight mission. We then re-evaluate existing literature models using a common, updated dataset and methodology to determine whether or not these models are consistent with current constraints on the composition and properties of Mars. Lastly, we leverage the most recent compilations of isotopic data and the associated bulk chemical compositions of various classes of meteorites to compute the bulk composition, and, in turn, internal structure of Mars. Extending the stochastic method of Liebske and Khan (2019), we (1) select the mixtures of meteorites that satisfy the observed isotopic composition of Mars, (2) determine whether such mixtures yield chemical compositions whose geophysical properties are consistent with Mars's mantle and core structure and thermal state as seen by the InSight mission, including updated observations of its astronomic-geodetic response, and (3) evaluate whether moderately volatile element abundances are in line with those observed on its surface. Our results indicate an apparent difficulty in assembling Mars from known meteoritic material, unless they have been chemically modified during accretion, thereby offering clues to the nature of the missing building blocks.

2. Compositional and building block models of Mars

2.1. SNC-based compositional models

Modern estimates for the composition of Mars date from the general recognition that the family of achondritic meteorites, that includes shergottites, nakhlites and chassignites (SNC), originated from Mars (McSween and Stolper, 1980); also see Stolper and McSween (1979), McSween et al. (1979), Wasson and Wetherill (1979) and Walker et al. (1979). These SNC-based models focused on the composition of the Martian primitive mantle and relied on geochemical relationships among SNC meteorites along with various cosmochemical assumptions, notably that refractory elements were present in CI carbonaceous chondrite relative proportions (Dreibus and Wänke, 1985, 1984; Wänke and Dreibus, 1988; Longhi et al., 1992; Wänke and Dreibus, 1994; Taylor and McLennan, 2009; Taylor, 2013). Although details differ, compared to Earth, all such models (collectively termed W-D models) indicate that Mars' primitive mantle is enriched in Fe (~18 wt% FeO), implying a more oxidised planet compared to Earth with a proportionately smaller metal core, and is volatile element enriched (e.g., has a high K/Th ratio), but still highly-depleted relative to most chondritic meteorites.

In a variant of the W-D approach, Yoshizaki and McDonough (2020) estimated the composition of Mars using geochemical relationships among SNC meteorites but without the assumption that refractory elements occur in CI proportions. They developed models for the primitive mantle and core independently, the latter being based largely on cosmochemical inferences (e.g., sulfur volatility) and geophysical properties (e.g., mean planet density and moment of inertia). This resulted in a core with a radius and mean density of 1580 km and 6910 kg/m^3, respectively, representing ~18% of the planet's mass, in contradiction with more recent estimates from the Mars InSight mission (Stähler et al., 2021; Khan et al., 2022; Lognonné et al., 2023; Irving et al., 2023). Their primitive mantle composition is broadly comparable to W-D, but with lower iron content (~14 wt% FeO). Their estimate for the bulk composition of Mars, however, differed from CI chondrites for certain key major element ratios (e.g., Fe/Si, Fe/Al).

Combining geophysical data from InSight with a cosmochemical model to estimate the composition of Mars, Khan et al. (2022) also concluded that its total FeO content was lower (13.6 wt%) than suggested by the W-D models but that, while highly depleted in moderately volatile elements (MVE) compared to most chondritic meteorites (i.e., lower K/Th), the level of depletion was not as great as suggested in either the W-D models or by Yoshizaki and McDonough (2020).

2.2. Meteorite mixing models

An alternative but highly complementary approach for evaluating the composition of Mars is to constrain the nature of the precursor materials that were assembled to make the planet. In general, such models evaluate proportions of known meteoritic material required to replicate the nucleosynthetic isotopic composition of SNC meteorites as being representative for Mars. However, prior to the recognition that SNC meteorites came from Mars, models estimating the bulk composition were mostly designed to meet the available geophysical constraints, notably size, density and mean normalised moment of inertia (MoI) (e.g., Anderson, 1972; Johnston et al., 1974; Johnston and Toksoz, 1977; McGetchin and Smyth, 1978). In a pioneering study, Anderson (1972) suggested two meteorite-based compositional models to explain the MoI then available (0.377; Binder, 1969): (1) a simple mixture of carbonaceous (75%) and ordinary (25%) chondrites and (2) partially differentiated ordinary chondrites.

The first attempts to constrain the potential meteoritic provenance of Mars through isotopic data were based on oxygen (Delaney, 1994; Lodders and Fegley, 1997; Sanloup et al., 1999; Burbine and O'Brien, 2004), but more recent studies have used additional isotopic compositions of elements that have emerged over the past two decades (Warren, 2011; Fitoussi et al., 2016; Brasser et al., 2018; Liebske and Khan, 2019; Dauphas et al., 2024). Such 'meteorite mixing' models can be grouped into those that considered differentiated bodies, the achondrites (e.g., EPB-eucrite parent body (4-Vesta), APB-angrite parent body as representatives), as a potential building block (Fitoussi et al., 2016; Liebske and Khan, 2019; Dauphas et al., 2024) and those that do not (Brasser et al., 2018; Dauphas et al., 2024). Warren (2011) combined all non-carbonaceous meteorites (ordinary and enstatite chondrites, differentiated achondrites) into one group (NC) and concluded that Mars most likely consisted of only about 9% carbonaceous chondrites (CC), with an upper limit of 30%, in a NC-CC mixture. In general, when included, differentiated parent body components are typically a major or even dominant component. In cases that consider only undifferentiated building blocks, enstatite chondrites tend to be more important.

In recognition of the non-uniqueness of isotope-based mixing models, Liebske and Khan (2019) used a broad range of isotopic and (pre-InSight) geophysical constraints on meteorite mixing models. They further considered varying distribution of Fe between core and mantle and allowed for differentiated achondritic bodies (APB, EPB) as potential building blocks. Their results confirmed the inherent non-uniqueness of relying solely on isotope mixing models. Adding the geophysical constraints further demonstrated that meteorite isotope mixing models based on chondrites were inconsistent with the geophysical constraints of Mars, mainly because they had too large cores, and

Table 1

Building block models for Mars. Abbreviations: Ordinary Chondrites (OC): H = H-chondrites; L = L-chondrites; LL = LL-chondrites; Enstatite Chondrites (EC): EH = High-Fe enstatite chondrites; EL = low-Fe enstatite chondrites; Carbonaceous Chondrites (CC): CI, CM, CV, CO; Achondrites (AC): APB = Angrite parent body; EPB = Eucrite parent body (Vesta). Abbreviations are used in the figures below.

Reference	Abbreviation	OC (%)	EC (%)	CC (%)	AC (%)	Primary basis of model
Anderson (1972); Model 1	A1	25	–	75	–	Match geophysics
Anderson (1972); Model 2	A2	100	–	–	–	Match geophysics
Delaney (1994)	De	90(H)	–	10(CM)	–	O-isotope and Fe-Mn-Mg mixing
Lodders and Fegley (1997)	LF	85(H)	–	11(CV); 4(CI)	–	O-isotope mixing
Sanloup et al. (1999); Model 1	S1	30(H)	70(EH)	–	–	O-isotope mixing
Sanloup et al. (1999); Model 2	S2	55(H)	45(EH)	–	–	O-isotope mixing
Mohapatra and Murty (2003)	MM	26	74	–	–	O-, N- and Cr-isotope mixing and Fe/Si
Burbine and O'Brien (2004)[a]	-[b]	55	16	26	–	O-isotope and major element mixing
Warren (2011)	W	-[c]	-[c]	9	-[c]	Stable isotope mixing
Fitoussi et al. (2016)	F	36(H)	–	9(CI)	55(APB)	Stable isotope mixing and bulk compositions
Brasser et al. (2018)	B	32	68	±3(CI); ±3(CV+CO)	–	Stable isotope mixing; assumes heterogeneous accretion
Liebske and Khan (2019)	LK	40(LL)	30(EH)	10	20(APB)	Stable isotope mixing and geophysics
Dauphas et al. (2024); Model 1	D1	33	65	2(CI+[CO+CV])	–	Stable isotope mixing; assumes heterogeneous accretion
Dauphas et al. (2024); Model 2	D2	37.8	10	12(CI); 2(Other C)	38.6(APB)	Stable isotope mixing; assumes heterogeneous accretion

[a] Also includes 14.4% R-chondrites; does not add up to 100% due to rounding; detailed components include: OC: H (12.3%), L (15.1%), LL (16.6%); EC: EH (7.8%), EL (8.3%); CC: CH (6.7%), CR (5.7%), CM (3.2%), CV (2.7%), CI (2.5%), CO (2.4%), CK (2.2%).

[b] Not plotted below, because the components R, CH, CR, and CK are not considered in this study.

[c] All non-carbonaceous meteorites were included in one group (NC) and the favoured model is for this component to represent 91% of Mars. In plots below NC was calculated as consisting of equal parts OC and EC.

that inclusion of relatively oxidised differentiated bodies with higher FeO/Fe ratios or smaller cores, such as APB and/or EPB, was required.

Table 1 lists most of the available models that have attempted to identify and quantify the various building blocks of Mars and three features stand out: (1) apart from ordinary chondrites being a component in all models (26%–90%, excluding Anderson, 1972), there is a remarkably wide variation in both the nature of the building blocks and their relative proportions; (2) carbonaceous chondrites play, at most, a minor role, with estimates ranging from 0% and up to 26% but mostly ≤15%. Where carbonaceous chondrites do appear in the models, the contribution of CI versus other classes (CM, CV, CO, etc.) is also variable; (3) for models that consider the APB and/or EPB (i.e., achondritic meteorite parent bodies) as a potential provenance component, it represents a significant but variable component (20%–55%).

3. Complementary geochemical and geophysical constraints

The considerable range in proposed meteorite classes and their relative proportions in the existing models, even restricting discussion to those from the past two decades, must give rise to a question of whether additional constraints need to be deployed in order to arrive at anything close to a unique solution. In our judgement, three additional types of constraints should be explicitly included in any models for the construction of Mars, (i) the nature of volatile-element depletion, (ii) the major element composition, and (iii) the most recent geophysical data, based on the InSight mission.

3.1. Constraints from moderately volatile elements

A ubiquitous feature of bodies in the inner solar system is the variable depletion of MVE (e.g., K, Na, Mn, Rb, Cs, Cu, Zn) compared to most chondritic meteorites (notably CI, ordinary and enstatite chondrites (e.g., Ganapathy and Anders, 1974; Jagoutz et al., 1979; Wänke, 1981; Taylor, 2001; Dauphas et al., 2022). From a planetary perspective, MVE abundances are best characterised geochemically by the K/Th ratio since K is moderately volatile, Th is refractory, both are lithophile and highly incompatible, and both can be measured on a planetary scale by gamma-ray spectroscopy. K/Th ratios for differentiated bodies in the inner solar system are as follows: Mercury ∼8300; Mars ∼5300; Earth ∼2600; 4-Vesta or Eucrite Parent Body (EPB) ∼900; Moon ∼650; Angrite Parent Body (APB) ∼35; which compares to the average CI value of about ∼18,000 and range of average ordinary and enstatite chondrites of ∼19,000 (H) to ∼29,000 (EH) (Lodders, 2023).

The nature of MVE-depletion on Mars was first characterised by Wänke and colleagues through geochemical studies of SNC meteorites (e.g., Wänke and Dreibus, 1988; Dreibus and Wänke, 1984). They documented SNC meteorite K/La ratios (La also being refractory and incompatible) that were nearly constant and differed from both Earth and most chondritic meteorites, which they attributed to the Mars primitive mantle being relatively enriched in MVE compared to the Earth (but still depleted compared to chondritic meteorites). Their analysis further predicted a Martian primitive mantle K/U of ∼19,000 and K/Th of ∼5400. The average Martian surface measurement of K/Th = 5330 ± 220 by the Mars Odyssey gamma-ray spectrometer experiment was a remarkable confirmation of these predictions.

The standard interpretation is that such depletions result primarily from evaporation–condensation processes taking place early in solar system history and are a fundamental property of planetary building blocks (e.g., Yin, 2005; Hu et al., 2023). An important exception is that low lunar, and possibly the low Vestan, K/Th values partly may result from volatility-related processes taking place during and/or in the aftermath of very large impacts (Sossi et al., 2019; Charnoz et al., 2021; Hu et al., 2023). On the other hand, Tian et al. (2021) proposed that there is a correlation between δ^{41}K and the surface gravity (i.e., size) for the terrestrial bodies Earth, Mars, Moon and 4-Vesta, suggesting that MVE-depletion was caused by volatility processes associated with planetary accretion rather than being inherited from precursor bodies. However, for plots of K/U (or K/Th) versus planetary size there is no such correlation with Mars notably having significantly higher levels of MVE than predicted from the K-isotope versus planetary size trend, by a factor >2. To explain this discrepancy, Tian et al. (2021) proposed that the surface of Mars is greatly enriched in potassium due to various geological processes and the near-surface K/Th (measured by GRS) is not representative of the bulk planet. We find this interpretation unconvincing for at least three reasons:

1. More recently obtained K-isotope results for angrites do not fall anywhere close to the suggested δ^{41}K vs. size trend (Hu et al., 2023) unless the APB is orders of magnitude more massive than 4-Vesta, which is unlikely (Keil, 2012);
2. Although Taylor et al. (2006) identified several geological processes that could fractionate K from Th in the near-surface environment of Mars, the important conclusions of that study were that K/Th was remarkably uniform across the planet, following a gaussian distribution with 95% of the surface falling in the narrow range of K/Th = 4000–7000, and was also fully consistent with being inherited from igneous rocks;

3. Extensive exploration by Mars rovers has identified aqueous alteration and other secondary processes that might influence K abundances but igneous compositions can be readily explained by conventional magmatic fractionation (e.g., McSween, 2015), and most sedimentary materials reflect underlying igneous provenance overprinted only by limited aqueous alteration processes (McLennan et al., 2019).

Our judgement is that the average near-surface Martian K/Th ratio, measured by GRS and largely confirmed by analyses on available magmatic rocks in the form of Martian meteorites (Udry et al., 2020), is indeed reflective of the bulk planet's composition and was largely inherited from the precursor bodies that accreted to form Mars. Accordingly, we consider the degree of moderately volatile element depletion to be an important constraint that should be applied when evaluating meteorite mixing models for the assembly of Mars. The average K/Th ratio derived from global gamma-ray mapping of the surface is 5330 ± 220 at 1-sigma (Taylor et al., 2006), and is broadly consistent with the highly variable Mars meteorite data (Udry et al., 2020). In adopting such a constraint, we allow for a substantially larger uncertainty window on K/Th of ± 500, equating to ~98.8% confidence level; i.e., K/Th = 4830–5830, which is also in the range of an updated GRS data analysis approach, but one that considered only the mid-latitudes (Rani et al., 2022) .

3.2. Major element constraints

Caution is required when attempting to use major element compositions to constrain the nature of Martian building blocks. In general, models for the composition of the silicate portion of terrestrial planets often call for chondritic relative proportions for refractory elements (e.g., Taylor, 2001) and so it is important to avoid circular arguments. For Mars, important elements to consider are Al, Mg and Si. Of these, Al is the most refractory, followed by Mg and then Si and so there is certainly some possibility that the key ratios Al/Si and Mg/Si are likely not in CI relative proportions (see Yoshizaki and McDonough, 2020; Khan et al., 2022).

Three major models for bulk silicate Mars described below each treat the major elements in somewhat different ways. The W-D models (most recently summarised by Taylor, 2013) are fundamentally based on the compositions of Martian meteorites but do assume chondritic (CI) relative proportions for the refractory elements (in which they include Al, but also Mg and Si, which are not strictly refractory elements according to their 50 % nebular condensation temperatures). On the other hand, Yoshizaki and McDonough (2020) base their compositions solely on elemental relationships among Martian meteorites and do not impose any explicit assumptions about chondritic proportions for refractory elements. Finally, Khan et al. (2022) impose both geophysical and cosmochemical constraints and, although they assume chondritic relative proportions for the most refractory Ca and Al (whose ratios are indeed constant to within 5 % among all chondrites), they also allow fractionation in Mg/Si and Fe/Si beyond the range observed in chondrites, provided their coupled variation follows the trend defined by chondrites, and the geophysical constraints are met.

In spite of these different approaches, the key major element ratios Mg/Si and Al/Si are remarkably similar across the three aforementioned studies (individual values given in Table 2) providing some confidence that the composition of Mars likely falls within the ranges provided by these models. We therefore average their Mg/Si and Al/Si ratios to obtain their most probable values, which are reported in Table 2 with propagated uncertainties. Within this parameter space (i.e. Mg/Si vs. Al/Si as will be shown below) these three proposed compositions for Mars are within fields defined by the major groups of chondrites, suggesting that, in principle, Mars might be explained by simple mixing among chondrites, contrary to Earth which appears to be an endmember (e.g. Drake and Righter, 2002).

3.3. Geophysical constraints

Geophysical studies, which, prior to InSight, mainly considered mean density, MoI, and possibly tidal response as geophysical constraints, have principally relied on predicting the geophysical response of bulk chemical models of Mars derived from either geochemical or isotope mixing analyses (e.g., Mocquet et al., 1996; Sohl et al., 2005; Verhoeven et al., 2005; Zharkov and Gudkova, 2005; Rivoldini et al., 2011; Wang et al., 2013; Zheng et al., 2015; Khan et al., 2018; Bagheri et al., 2019; Smrekar et al., 2019) or independently-determined compositions (Khan and Connolly, 2008). Based on the bulk chemical Martian models of Dreibus and Wänke (1985), Lodders and Fegley (1997), Sanloup et al. (1999), Taylor (2013), the study of Khan et al. (2018) demonstrated that changes to e.g., bulk Fe/Si ratio, core sulfur content, and/or core size were needed for these models to match the geophysical constraints. Ultimately, this implies that none of the bulk chemical models, whether derived from mixing models or from geochemical considerations, are able to self-consistently explain major element chemistry, isotopic composition, and geophysical properties simultaneously.

Since then the InSight mission has provided a series of new constraints on the interior structure of Mars. Of particular interest here is the observation of a liquid core with a radius and density in the ranges of 1780–1870 km and 6–6.3 g/cm^3, respectively (Durán et al., 2022; Drilleau et al., 2022; Irving et al., 2023). This large, low-density Fe-rich core has subsequently been revised in view of evidence indicating that the outermost part of the core may in fact represent the bottom of the mantle in the form of a liquid silicate layer of about 135–165 km thickness, reducing core size to 1645–1705 km, while increasing density to 6.55–6.75 g/cm^3 (Khan et al., 2023, see also Samuel et al., 2023). In addition, InSight showed that Mars has a lithosphere with a thickness in the range 400–500 km (Khan et al., 2021; Durán et al., 2022; Drilleau et al., 2022), which is supported by the observation of a single-plate planet with low levels of seismicity (Stähler et al., 2022; Ceylan et al., 2023). Based on thermodynamic considerations, data, and models, the InSight seismic data were also found to be compatible with elevated mantle temperatures, corresponding to mantle potential temperatures in the range 1700–1850 K (Khan et al., 2023). In summary, we argue that any model of Mars derived from either geochemical considerations or isotopic mixing models must be compatible with the large-scale seismic structure of Mars derived from InSight, in particular core size and density and thus core mass fraction. The geophysical observations are summarised in Table 3.

Although we rely on the most recent core radius and mean density determined by InSight, we should note that this is based on the observation of a single far side impact (Posiolova et al., 2022), which produced the only clear observations of seismic waves interacting with the core-mantle-boundary and traversing the liquid core (Horleston et al., 2022; Durán et al., 2022; Irving et al., 2023). On account of the dearth of supporting observations, the interpretation of the seismic phases associated with the far side event, however, is non-unique (see e.g., Durán et al., 2022, for an alternative solution). Yet, the initial interpretation of a large low-density core (Stähler et al., 2021; Irving et al., 2023) faced a number of objections that are not easily overcome: (1) a large, molten core with a low mean density implies a light element budget (of which S is the most important) in excess of 20 wt% in contradiction with their availability in the potential building blocks of the terrestrial planets (Brennan et al., 2020; Khan et al., 2022) and (2) the core density deficit relative to pure liquid Fe is nearly 30%, i.e., three times that of the Earth's, whereas the P-wave velocity is almost equal to that of pure liquid Fe (Irving et al., 2023; Huang et al., 2023; Khan et al., 2023). The latter observation clearly indicates that, in addition to S, other light elements (e.g., C, O, H) are present in Mars' core. The alternative model, consisting of a fully molten mantle layer surrounding a smaller and denser liquid Fe core, addresses both of these

Table 2
Major, minor and trace elements of chondritic and achondritic endmembers. Chondritic endmembers are based on (Lodders, 2023). See text for details. Missing values are assumed zero in geochemical mixing models.

	CI	CM	CV	CO	H	L	LL	EH	EL	ABP	EPB
Silicate mantle											
SiO_2	25.11	29.44	33.58	33.88	36.33	39.27	40.12	35.12	40.56	30.3	36.8
TiO_2	0.08	0.11	0.14	0.13	0.1	0.11	0.11	0.08	0.09	0.16	0.48
Al_2O_3	1.72	2.25	3.15	2.65	2.09	2.2	2.21	1.57	1.94	3.0	2.94
Cr_2O_3	0.42	0.47	0.52	0.52	0.51	0.53	0.53	0.47	0.47	0.24	0.2
FeO	12.93	21.24	23.94	24.93	13.16	15.17	16.82	0	0	16.3	11.7
MnO	0.27	0.23	0.19	0.21	0.3	0.33	0.33	0.28	0.21		0.3
MgO	17.19	20.57	24.07	24.1	23.04	24.5	25.17	18.41	23.25	26.2	25.4
CaO	1.35	1.75	2.49	2.2	1.73	1.81	1.83	1.22	1.41	2.8	2.5
Na_2O	0.75	0.56	0.45	0.55	0.82	0.92	0.92	0.97	0.82	0.002[b]	0.04[b]
K_2O	0.07	0.05	0.04	0.04	0.09	0.11	0.1	0.1	0.09		
P_2O_5	0.24	0.23	0.25	0.26	0.27	0.23	0.22	0.52	0.28		
Volatiles											
H_2O	18.11	10.71	2.47	0.9	0.71	1.12	1.51	0.58	0		
C	4.5	2.42	0.48	0.49	0.23	0.25	0.39	0.39	0.49		
Metal & sulfide											
Fe	0	0.03	1.05	1.68	13.35	6.12	2.94	21.86	19.42	10.6	9.1
FeS	16.01	8.57	5.74	5.99	5.46	6	5.71	15.72	9.13	9.1	7.8
Ni	1.19	1.3	1.38	1.41	1.7	1.26	1.01	1.91	1.55	1.3	1.1
Co	0.06	0.06	0.06	0.07	0.08	0.06	0.05	0.09	0.07	0.065	0.055
Si	0	0	0	0	0	0	0	0.72	0.21		
Traces (ppm)											
Sr	7.8	10	14.6	13.2	8.7	11	11	7.1	7.9	14.3[d]	12.2[d]
Mo	0.98	1.2	1.5	1.6	1.4	1.2	1.1	1	0.73	6.9[d]	5.9[d]
Zr	3.8	5.2	6.8	6	5.7	5.8	6.8	3.8	4.8	1[c]	1[c]
K	539	410	310	360	760	880	860	850	705	1.98[a]	57.5[a]
Th	0.03	0.042	0.059	0.046	0.04	0.04	0.046	0.029	0.031	0.057[a]	0.051[a]
K/Th	18 087	9762	5254	7826	19 000	22 000	18 696	29 310	22 742	35	1127
Mars											
K/Th[e]	5330 ± 500										
Mg/Si[f]	0.896 ± 0.048										
Al/Si[f]	0.085 ± 0.0070										

[a] Based on (Dauphas et al., 2022); for APB see text for details.

[b] Assumed 10 × K_2O.

[c] Estimated.

[d] Based on CI chondritic Al/Sr or Al/Zr ratios.

[e] After (Taylor et al., 2006); see Section 3.3 for discussion of uncertainty.

[f] The values quoted represent averaged values from Taylor (2013), Yoshizaki and McDonough (2020), and Khan et al. (2022) for which Mg/Si = 0.902 ± 0.052; 0.879 ± 0.133; 0.907 ± 0.017 and Al/Si = 0.080 ± 0.004; 0.089 ± 0.019; 0.084 ± 0.007, where uncertainties indicate 2σ.

issues (Khan et al., 2023, see Samuel et al., 2023, for a variant thereof) although the core light element budget remains relatively high.

The geophysical data that we consider here include mean planet density ($\bar{\rho}$) and mean normalised moment of inertia (I/MR^2), and second-degree tidal Love number (k_2), which measures the rigidity of the planet. Values adopted here for $\bar{\rho}$, I/MR^2, and k_2 are summarised in Table 3. Note that the observed tidal Love number in Table 3 has been corrected for anelastic contributions, following the approach described in Khan et al. (2014) and using a frequency exponent of 0.33 after (Bagheri et al., 2019), in order that it is representative of purely elastic effects. Based on InSight, we consider mean core mass fraction as a constraint, along with lithospheric and geothermal structure, which serve as input for the geophysical model (Section 4.3).

4. Data and methods

In the following we present our preferred chemical compositions of meteoritic endmembers in terms of major, minor and trace elements, including their nucleosynthetic isotopic signatures (Section 4.1), and explain the procedure to convert mixtures of the unmodified endmembers into hypothetical planets (Section 4.2) for which geophysical properties are predicted (Section 4.3).

4.1. Data selection: meteorite compositions

4.1.1. Major, minor and trace elements

The bulk chemical compositions for the different meteorite groups that are used as endmembers for mixing models were re-evaluated with respect to the values given by Liebske and Khan (2019), such that we now rely on the more recent compilation of Lodders (2023), rather than on Wasson and Kallemeyn (1988). This is well-justified because the Lodders compilation includes both new data on previously reported meteorites as well as data on new meteorites that have been added to the collection since 1988. Lodders (2023) does not provide a systematic error analysis for all of the meteorite classes (apart from CI) but notes that the precision for all abundances is <10% relative.

To estimate the silicate- and core components we first convert all available S to FeS, then the remaining Fe is assigned to silicate and metal. Since Lodders (2023) does not report the redox state of Fe, we use the average molar $Fe^0/(Fe^0 + FeO)$ ratio derived from the compilation of Jarosewich (1990) to distribute Fe between the two reservoirs. Other elements are recalculated as oxides, except Ni, Co and C. To account for the presence of Si-metal in the core-components of highly reduced E-chondrites, we reassign 3 and 1 wt% Si^0 to the metal fractions of EH and EL (estimates from Weyrauch et al., 2018), respectively, and correct for the appropriate amount of SiO_2 in the silicate. Finally all compositions are normalised to 100%. Bulk composition estimates for APB and EPB are adapted from Liebske and Khan (2019), but the mantle composition of APB is updated with the recent estimate of Tissot et al. (2022). All compositions are summarised in Table 2.

The K and Th concentrations for chondritic endmembers are also taken from Lodders (2023), and for the differentiated bodies from Dauphas et al. (2022). Note, that Dauphas et al. (2022) only report K and Th concentrations for the Angra dos Reis (ADOR) meteorite because it is the only observed fall among angrites, whose K content

Table 3
Summary of Martian geophysical data and observations, uncertainties, and sources. k_2 refers to the main solar tidal period of 12 h 19 min. GM for Mars, where G is the gravitational constant and M Mars's mass, is 42 828.3758 ± 0.0002 km^3/s^2 based on gravity field MRO120F from Mars Reconnaissance Orbiter (Konopliv et al., 2020) and CODATA 2018 (Tiesinga et al., 2021).

Observation	Symbol	Value (±uncertainty)	Source
Mean density	$\bar{\rho}$	3933.94 ± 0.089 kg/m^3	Le Maistre et al. (2023)
Mean moment of inertia	I/MR^2	0.36428 ± 0.00011	Le Maistre et al. (2023)
Tidal Love number[a]	k_2	0.171 ± 0.008	Konopliv et al. (2020)
Mean planet radius	R	3389.508 ± 0.003 km	Le Maistre et al. (2023)
Mean crustal thickness	d_{crust}	50 km	Kim et al. (2023)
Mean lithospheric thickness[b]	d_{lit}	425 km	Khan et al. (2023)
Mean base lithosphere temperature[b]	T_{lit}	1800 K	Khan et al. (2023)
Mean core density	ρ_{core}	6.65 ± 0.1 g/cm^3	Khan et al. (2023)
Mean core radius	R_{core}	1675 ± 30 km	Khan et al. (2023)
Mean core mass fraction	X_{core}	0.21	Khan et al. (2023)

[a] Elastically-corrected value.

[b] The estimates refer to the thermal lithosphere.

is believed to be the most pristine and not affected by terrestrial weathering, as might be suspected for finds (Dauphas et al., 2022). While the K/Th ratio of ADOR is presumably identical to that of the parent body APB, the absolute concentrations are likely enriched in the meteorite as a result of magmatic differentiation (ADOR is a nearly monominerallic clinopyroxenite Keil, 2012). Such an enrichment, if not corrected for, would have substantial consequences for mass balance on the K/Th ratio of endmember mixtures. To estimate the concentrations of the angrite parent body we assume a CI-chondritic Al/Th ratio, and use the Al concentration of APB given by Tissot et al. (2022) to scale Th to 0.057 ppm, which, with an angrite K/Th ratio of 35 (Dauphas et al., 2022), gives 1.98 ppm K in the APB. Note that the derived Th-concentration of the APB is of the same order of magnitude as in all other endmembers (0.03–0.06 ppm, see Table 2), whereas its abundance in ADOR is about 10× higher (∼0.5 ppm; Dauphas et al., 2022, derived from uranium), which supports our argument that the meteorite is enriched in incompatible elements relative to the parent body.

4.1.2. Isotopic anomalies

Estimates for the isotopic compositions among meteorite groups are taken from the compilation provided in Dauphas et al. (2024) (Table 4), which are themselves derived from a wide variety of sources (e.g., Zhang et al., 2012; Schiller et al., 2018; Budde et al., 2019; Burkhardt et al., 2021; Akram and Schönbächler, 2016; Bermingham et al., 2018; Charlier et al., 2019; Yokoyama et al., 2019; Williams et al., 2021; Zhu et al., 2022; Kruijer et al., 2020; Render et al., 2022; Rüfenacht et al., 2023; Torrano et al., 2021). The array of compositions now available spans the range of geochemical properties of the elements, which, roughly ordered from most- to least-lithophile are: Ca∼Sr∼O∼Ti∼Zr>Cr>Ni>Mo. Any differences in the inferred mixture of chondritic components as a function of the degree of siderophile character of the element has been used as the basis to argue for heterogeneous accretion (Dauphas, 2017; Kleine and Nimmo, 2024).

Moreover, recent studies on the isotopic composition of Nd (not included here due to its limited isotopic spread among planetary materials) illustrate that the Earth is an endmember among the group of meteorites, being typified by an enrichment in isotopes produced by the s-process (see also Burkhardt et al., 2016; Bouvier and Boyet, 2016). Consequently, this endmember status was shown to extend to other nuclides heavier than Fe, namely, Mo, Zr, and Ru (Budde et al., 2016; Fischer-Gödde et al., 2020; Render et al., 2022; Rüfenacht et al., 2023), indicating that the isotopic anomalies expressed in these elements originate entirely from differences in the nucleosynthetic pathways by which they were made. Insofar as these anomalies cannot be generated by mass transfer within a closed system (e.g., planetary differentiation), we take these ratios as indicative of the provenance of the source material constituting Mars. One exception is the isotope composition of O, whose variability is also related to irradiation in the early Solar System owing to its volatile nature and hence residence in the gas phase as H_2O and CO (Lyons and Young, 2005).

4.2. The geochemical model

The chemical compositions of mixtures of chondrites and achondrites are calculated as follows. The concentration c_i of a chemical component m (i.e., oxides or elements) in a mixture (c^m_{Mix}) of N meteoritic endmembers with their respective mass fractions x_i is calculated from

$$c^m_{\text{Mix}} = \sum_{i=1}^{N} x_i \cdot c^m_i. \tag{1}$$

Similarly, the standard-normalised ratio of an isotopic anomaly of element m with mass τ, expressed as ϵ, μ or Δ depending on a scaling factor (see Table 4), is derived from (taking ϵ as example),

$$\epsilon^\tau m_{\text{Mix}} = \frac{\sum_{i=1}^{N} x_i \cdot c^m_i \cdot \epsilon^\tau m_i}{c^m_{\text{Mix}}}. \tag{2}$$

The mass fractions x_i are either taken from the previous building block models listed in Table 1, or by randomly generating them using the procedure outlined by Liebske and Khan (2019) for the purpose of exploring the range of mixture that can isotopically produce a Martian signature (see Section 5.2). In the latter approach we account for the uncertainty in the isotope data by calculating each random mixture 250 times and imposing a gaussian distribution on each endmember isotope value, such that ∼95% of the random draws fall within the uncertainty of the isotopic average. To identify mixtures representative of Mars based on isotopic constraints, we then filter the results using the target values listed in Table 4. Any mixture that produces an isotopic signal consistent within the range of uncertainty is considered a match. Finally, any duplicates in the matching mixtures are eliminated to obtain unique solutions. This approach samples the entire range of mixtures that are statistically consistent with Mars, but it is different compared to methods applied by Dauphas et al. (2024) or Fitoussi et al. (2016) which converge towards unique solutions by considering misfit parameters.

The chemical compositions of mixtures with respective core, mantle and volatile reservoirs are then calculated from Eq. (1) and endmember compositions reported in Table 2, and we assume that each reservoir mixes homogeneously. Such mass balanced chemical compositions may not be in chemical equilibrium with each other and thus can undergo redox reactions, in particular due to the presence of the volatile species H_2O and C, which can alter the bulk redox state, mainly by affecting the core-mantle distribution of Fe and FeO. Modelling appropriate reactions requires a more rigorous thermodynamic treatment, and specifying pressure, temperature and oxygen fugacity during accretion (e.g., Rubie et al., 2015). Such an approach is beyond the scope of this paper, however, as done our previous study (Liebske and Khan, 2019) we envisage the maximum amount of core oxidation or mantle reduction through H_2O and C, respectively, through the following reactions:

$$Fe_{\text{core}} + H_2O = FeO_{\text{mantle}} + H_2 \tag{3}$$

Table 4

Summary of isotopic anomalies taken from the recent study of Dauphas et al. (2024).

	Δ^{17}O	±	ϵ^{48}Ca	±	ϵ^{50}Ti	±	ϵ^{54}Cr	±	ϵ^{64}Ni	±	μ^{84}Sr	±	ϵ^{92}Mo	±	Δ^{95}Mo	±	μ^{96}Zr	±
CI	0.41	0.11	2.07	0.07	1.91	0.06	1.47	0.09	0.62	0.1	42	31	0.97	0.45	56	30	83	16
CM	−2.92	0.44	3.13	0.14	2.95	0.1	0.98	0.06	0.37	0.09	49	9	5.67	0.81	32	15	104	22
CO	−4.32	0.26	3.87	0.56	3.41	0.35	0.84	0.13	0.26	0.11	49	15	2.02	0.63	15	28	84	21
CV	−3.62	0.48	2.51	0.02	3.35	0.14	0.91	0.03	0.31	0.04	71	8	1.8	0.07	33	7	114	13
H	0.72	0.05	−0.15	0.26	−0.57	0.09	−0.38	0.02	−0.16	0.05	2	38	0.86	0.19	−14	6	44	14
L	1.03	0.04	−0.14	0.02	−0.63	0.02	−0.32	0.1	−0.11	0.06	4	14	0.69	0.24	−15	14	34	13
LL	1.19	0.06	−0.36	0.05	−0.65	0.03	−0.42	0.05	−0.18	0.05	−15	15	0.77	0.3	−16	8	30	4
EH	−0.03	0.1	−0.11	0.02	−0.12	0.03	0.04	0.05	0.14	0.11	−14	13	0.48	0.33	−11	9	15	6
EL	−0.01	0.07	−0.18	0.04	−0.31	0.06	0.04	0.05	−0.05	0.07	6	25	0.37	0.09	−7	5	17	7
APB	−0.11	0.11	−1.04	0.18	−1.15	0.02	−0.43	0.05	0.09	0.07	−2	9	0.47	0.57	−6	9	50	5
EPB	−0.29	0.08	−1.21	0.23	−1.23	0.03	−0.67	0.07	0.18	0.1	−7	8	0.47[a]	0.86	−6[a]	13	39	8
Mars	0.27	0.03	−0.2	0.02	−0.44	0.04	−0.17	0.03	0.14	0.1	−27	12	0.57	0.08	5	5	27	2

[a] Not given by Dauphas et al. (2024), and estimated to be identical to APB with 50% increase in uncertainty.

and

$$2\mathrm{FeO}_{\mathrm{mantle}} + \mathrm{C} = 2\mathrm{Fe}_{\mathrm{core}} + \mathrm{CO}_2. \tag{4}$$

Furthermore, core-mantle redox reaction may occur through oxidation of Si metal that is present within the EC components (c.f. Table 2) according to

$$\mathrm{Si}_{\mathrm{core}} + 2\mathrm{FeO}_{\mathrm{mantle}} = \mathrm{SiO}_{2,\mathrm{mantle}} + 2\mathrm{Fe}_{\mathrm{core}}. \tag{5}$$

Lastly, taking into account that Mars' accretion may have involved a magma ocean stage implies that hydrogen, carbon and oxygen, among the elements which have the most significant effect on core density next to sulfur, may have partitioned between silicate melt and core-forming liquids. The boundary conditions under which these elements can enter core-liquids in sufficient amounts are discussed elsewhere (e.g. Brennan et al., 2020; Steenstra and van Westrenen, 2018; Khan et al., 2022), and below we qualitatively access their principal effects on bulk planets geophysical properties when dissolved into the core (Section 6.2).

To convert the isotopically matching mixtures into model compositions for which geophysical properties can be calculated, core and mantle constituents need to be recalculated as mantle oxide components in the NCFMAS model chemical system comprising the oxides Na_2O-CaO-FeO-MgO-Al_2O_3-SiO_2, and Fe and S in the core for compatibility with the geophysical model (Section 4.3). All oxides listed in Table 2 are assigned as mantle components, and molar proportions of minor elements not included in NCFMAS are reassigned to major elements according to valence state, respectively, e.g., TiO_2 is recalculated as SiO_2, similarly Cr_2O_3 as Al_2O_3. Since H_2O and C are not considered in the geophysical model they are assumed to be lost during accretion, but we note that reactions such as (3) and (4) may cause a permanent redox change to a planet if volatile reaction products escape to space. The consequences of such processes for the geophysical properties of a planet are qualitatively assessed in Section 6.2. For the core we assume that any Si metal from EC components is oxidised through reaction (5) to SiO_2 and further, Fe and Ni and Co are recalculated in their respective molar proportions as Fe, to simplify the core system to Fe-S.

4.3. *The geophysical model*

In converting a Martian geochemical composition via mass balance considerations (Section 4.2) into a geophysical model, we rely, as in our previous work, on phase equilibrium computations to compute radial seismic properties (e.g., P- and S-wave speed and density) of the mantle and equation-of-state modelling for core properties. Martian compositions are explored in the Na_2O-CaO-FeO-MgO-Al_2O_3-SiO_2 model chemical system, which accounts >99% of the mass of the Martian mantle (Bertka and Fei, 1998). We further assume that the Martian mantle mineralogy and physical properties are governed by thermodynamic equilibrium and computed for a given model pressure, temperature, and bulk composition along a temperature profile by Gibbs free-energy minimisation (Connolly, 2009) using the thermodynamic formulation and parameters described in Stixrude and Lithgow-Bertelloni (2005) and Stixrude and Lithgow-Bertelloni (2011).

To model the thermal state of the Martian mantle, we consider the average thermal profile of Khan et al. (2023), based on InSight results. Because of uncertainties in the Martian temperature profile, the effect of the assumed parameters on the computed geophysical data were tested by running a composition using the "coldest" and the "hottest" temperature profile obtained by Khan et al. (2023). At the pressure–temperature conditions of Mars's mantle, the computed density and elastic moduli are uncertain by ∼0.5% and ∼1–2%, respectively (Connolly and Khan, 2016). The resultant uncertainties in geophysical responses are illustrated for a single composition (H chondrite) in Fig. 1b (grey trapezoidal region under symbol "H"). For the crust, we consider the average crustal composition of Taylor and McLennan (2009) and assume a mass fraction of 0.05, corresponding to a crustal thickness of 50 km in line with the average Moho depth of the planet as seen by InSight (Durán et al., 2022; Kim et al., 2022, 2023). The main model parameters are summarised in Table A.1. The mantle pressure profile is obtained by integrating the vertical load from the surface pressure boundary condition.

For the core, we follow our earlier study (Liebske and Khan, 2019) and recalculate the core composition to be a binary mixture of Fe-S (see Section 4.2), which is entirely liquid, well-mixed, and convecting. This parameterisation is a simplification given evidence that S is unlikely to be the sole light alloying element in Mars's core. Recent studies have shown that the Martian core must contain additional light elements, such as C, O, and H (e.g. Khan et al., 2022; Huang et al., 2023). Estimating the amounts of these elements in core liquids, however, requires modelling specific accretion paths, which is beyond the scope of this study. We therefore rely on S as a proxy for light elements in the core, which may be justified in view of the fact that of all the light elements, S is by far the most abundant (≥8 wt%), while C, O, and H are expected to be present at levels at the most of 0–2 wt% (Huang et al., 2023). The thermoelastic properties of liquid Fe and liquid Fe-S alloys are determined using the equations-of-state described in Khan et al. (2018). As this potentially limits the usefulness of mean core density as a constraint, we abstain from making a quantitative comparison with the core density derived from InSight and only seek a qualitative match. Model parameters are summarised in Table A.1.

Note that while core Fe and S content are input parameters for the geophysical model, they are not determined independently of the mantle composition, but are related to the FeO content of the latter through the exchange redox reactions (Eqs. (3)–(5)) discussed earlier. For example, an increase of one mole in mantle FeO is balanced by a decrease of one mole Fe in core mass in order to maintain a constant total Fe abundance in any given bulk composition. Mean mass and moment of inertia are computed by simple integration of the density profile. Finally, to determine the tidal response in the form of the degree-2 Love number, k_2, of a spherically symmetric, self-gravitating,

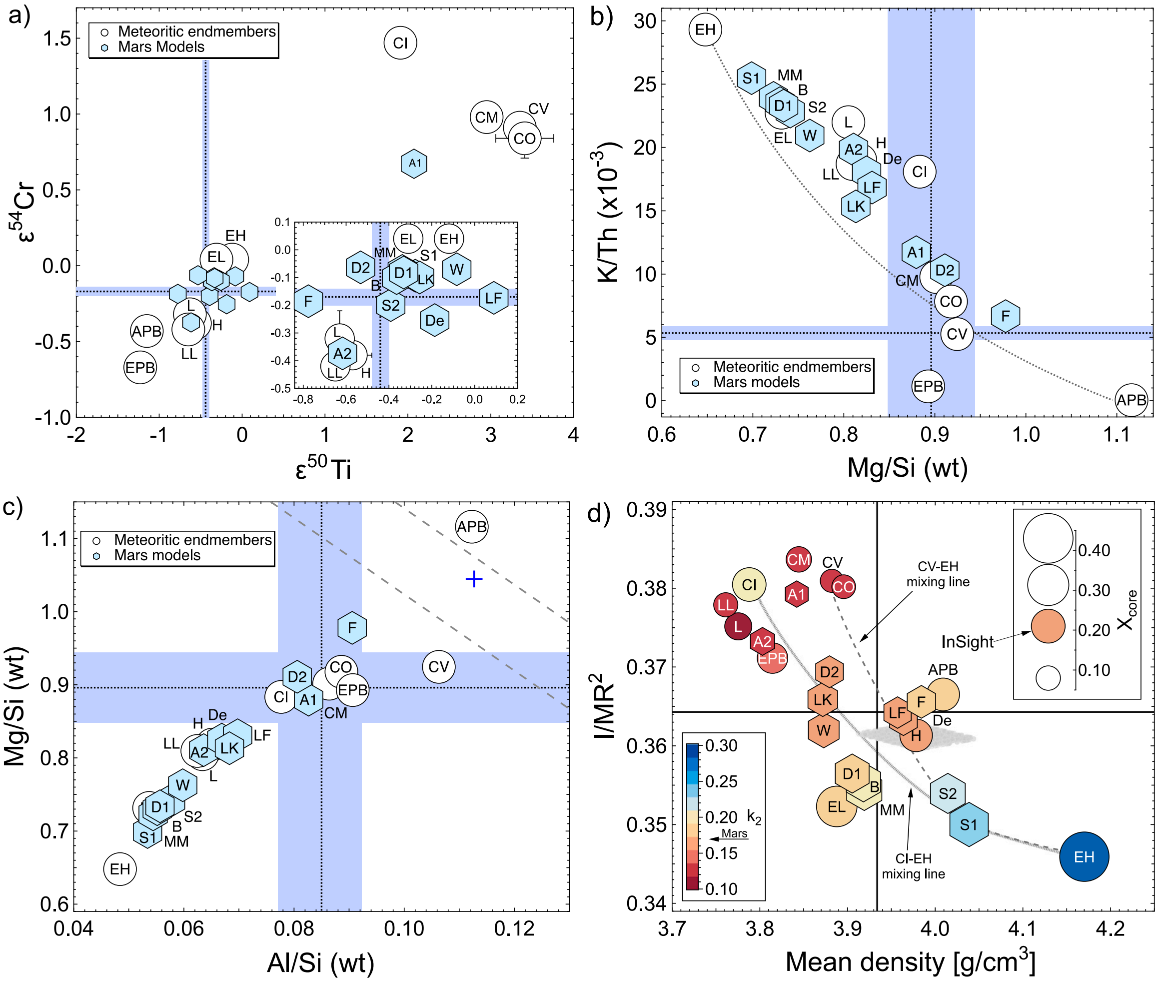

Fig. 1. Compilation of isotopic, geochemical and geophysical observations for chondritic- and achondritic end-members and published Mars models (see Table 1 for abbreviations) Meteoritic material includes undifferentiated ordinary (H, L, LL), carbonaceous (CI, CO, CM, CV) and enstatite (EH, EL) chondrites and achondrites (differentiated objects) in the form of angrites (APB) and eucrites (EPB). Horizontal and vertical lines and blue bars indicate observed Martian values and uncertainties, respectively. All Mars models are recalculated using data in Tables 2 and 4. (a) Nucleosynthetic isotope anomaly plot showing variation in ϵ^{54}Cr vs. ϵ^{50}Ti for the various meteoritic endmembers and Mars models considered here. (b) and (c) Moderately volatile (K/Th) and major element (Mg/Si, Al/SI) compositions of the various meteoritic endmembers and Mars models considered in this study. The blue cross in (c) is represents Earth's primitive upper mantle (Palme and O'Neill, 2003). (d) Predicted geophysical properties of endmembers and Mars models, including CI–EH and CV–EH mixing lines. Their convergence near EH is a consequence of Si oxidation from the core component of EH through FeO and H_2O of the carbonaceous components, effectively holding the mantle Mg# (molar Mg/(Mg+Fe)×100) constant at 100 for low carbonaceous chondrite fractions. "InSight" refers to the recent seismic determination of core mass fraction (Table 3). The grey area in panel d) indicates the uncertainty range in geophysical space, exemplified here for H chondrites. (For interpretation of colors the reader is referred to the web version of this article).

and viscoelastic planetary body, we solve the static momentum equation using a spectral element discretisation as described in more detail in Bagheri et al. (2019).

5. Results

5.1. Reassessment of building block models

In Fig. 1 we have summarised model results for the major meteorite classes expressed in their nucleosynthetic isotope anomalies (exemplified here using ϵ^{50}Ti and ϵ^{54}Cr), moderately volatile (K/Th) and major-element geochemistry (Mg/Si, Al/Si) and geophysics, in comparison with the reevaluated bulk Mars chemical models listed in Table 1. Compositions and isotope signatures for the models that only refer to meteorite classes (EC, OC CC), rather than individual groups, are calculated as non-weighted averages from the values reported in Tables 2 and 4.

We emphasise that, because all models are recalculated using data and applying the methodology outlined above, results may differ from those given in the original publications. Our purpose is not to question any of the previous studies, as all were bound to the available constraints at the time, but to evaluate common features through a consistent treatment. We mention and discuss cases where significant deviations between original and recalculated parameters arise. From Fig. 1 we can derive the following set of observations:

- We base our analysis on isotopic anomalies of the Martian meteorites, of which ϵ^{50}Ti versus ϵ^{54}Cr are shown in Fig. 1a. The choice of ϵ^{50}Ti and ϵ^{54}Cr is important because (i) Ti, in particular, is a refractory lithophile element, and therefore its composition must record an integrated history of Martian accretion, even in the event of heterogeneous delivery of material with different nucleosynthetic provenance (Dauphas, 2017), and (ii), the isotopic range among planetary materials is among the largest relative to analytical uncertainty (Trinquier et al., 2007), making both systems (i.e. Ti and Cr) an excellent means of fingerprinting the distinct origin of putative Mars-forming material. Considering these two systems in isolation, the carbonaceous chondrites can, at most, be only a minor component of Mars, whereas the ordinary and enstatite chondrites if mixed in near-equal proportions would appear to match Mars. Note, that in our reevaluation the most recent mixing models (D1, D2) from Dauphas et al. (2024)

do not exactly fit the target range indicated by the light blue vertical and horizontal bars, because we employ original isotopic data and not their statistically optimised values. However, given the available constraints at the time of publication, many models still plot reasonably close to Mars, except A1 from Anderson (1972), who had no isotopic data available.

- With the exception of CV, none of the chondrites match the geochemistry of the Martian mantle as inferred from the SNC meteorites in terms of both K/Th and Mg/Si (Fig. 1b). This result is in stark contrast to the inferred isotopic building blocks of Mars (Fig. 1a). Mixtures among other classes of ordinary and enstatite chondrites mostly require a major contribution from volatile-depleted bodies, most likely APB (Fitoussi et al., 2016; Dauphas et al., 2024). However, assuming that E-chondrites are an important constituent of Mars would require ∼70% of APB (dashed mixing line in Fig. 1b) to match constraints on Mg/Si and K/Th in conflict with the geophysical constraints shown below (see Fig. 1d). Fitoussi et al. (2016), whose mixture contains 55% APB, proposed a K/Th ratio of 5576 (see their Table 2), whereas our recalculated value is ∼6700, which is likely related to different assumptions regarding K and Th in the APB. Fitoussi et al. (2016) do not specify the concentrations of K and Th in their angrite endmember, however, their values are not based on angrites themselves but derived from a CV-chondrite composition following arguments of Jurewicz et al. (2004). Although the model of Fitoussi et al. (2016) comes closest to the target value in terms K/Th, their Mg/Si ratio is slightly too high and they are unable to meet the constraints imposed by the current isotopic data for Mars (Fig. 1a).
- While Earth is an endmember in Mg/Si vs. Al/Si space relative to chondritic bulk compositions, Mars is not (Fig. 1c), and, for these variables, its composition is consistent with a variety of combinations, either dominated by carbonaceous material (CI, CM, CO) and EPB, or containing OC, and EC material if compensated for by APB which lies closer to Earth. Clearly a large proportion of CC is excluded based on isotopic constraints. The model of Dauphas et al. (2024), on the other hand, matches major element constraints as they allow for ∼39% APB, although their model fails to match MVE abundances when adopting our K and Th concentration estimates for APB. Models that are dominated by OC and EC are too Si-rich relative to Mg and Al, and have K/Th ratios that are too high.
- Based on the geophysical characteristics shown in Fig. 1d, the H chondrites come closest to matching Mars and, as a consequence, models that are rich in this component (e.g., LF, De) are viable solutions in the I/MR^2 vs. mean density space, within error, but lie outside the Martian range for the remaining parameters (Fig. 1a-c). Next to H-chondrites, APB also lies in close proximity to Mars, and the model of Fitoussi et al. (2016), which consists predominantly of these two endmembers (see Table 1), may potentially represent a solution. We may note that the model of Liebske and Khan (2019) is offset to lower mean densities as a consequence of the revised APB composition.
- The enstatite chondrites, should they differentiate into core and mantle, would have too large cores, resulting in too high mean densities and low moment of inertia values, and therefore falling into the lower-right quadrant relative to Mars, while carbonaceous chondrites would have too small or too light cores, occupying the top-left quadrant in $\bar{\rho}$ vs. I/MR^2 space. The CI-EH mixing line illustrates that a mechanical mixture of the two is unable to match the geophysical observations. The CV-EH mixing line (dashed curve, Fig. 1d), although compatible with geophysical constraints, is inconsistent with the geochemical properties of Mars.

Table 5

Summary of stochastic meteorite mixing simulations and application of different isotopic filter sets (FS). No other compositional constraints are applied. For each model, 10^7 random mixtures were created and filtered for different sets of nucleosynthetic isotopes. *n* refers to the number of mixtures that match the isotopic signature of Mars.

Model	Considered isotopes	*n*
FS1	Δ^{17}O, ϵ^{48}Ca, ϵ^{50}Ti, ϵ^{54}Cr, ϵ^{64}Ni, μ^{84}Sr, ϵ^{92}Mo, Δ^{95}Mo, μ^{96}Zr	0
FS2	ϵ^{48}Ca, ϵ^{50}Ti, ϵ^{54}Cr, ϵ^{64}Ni, μ^{84}Sr, ϵ^{92}Mo, Δ^{95}Mo, μ^{96}Zr	0
FS3	Δ^{17}O, ϵ^{48}Ca, ϵ^{50}Ti, μ^{84}Sr, μ^{96}Zr	2245
FS4	Δ^{17}O, ϵ^{48}Ca, ϵ^{50}Ti, ϵ^{54}Cr, μ^{84}Sr, μ^{96}Zr	833
FS5	Δ^{17}O, ϵ^{48}Ca, ϵ^{50}Ti, ϵ^{54}Cr, ϵ^{64}Ni, ϵ^{92}Mo, μ^{96}Zr	852
FS6	ϵ^{48}Ca, ϵ^{50}Ti, ϵ^{54}Cr, ϵ^{64}Ni, ϵ^{92}Mo, μ^{96}Zr	6716

In conclusion, Fig. 1 serves to summarise the fundamental challenges of relying on the currently-available meteorite collection to define the building blocks for Mars, as the proposed models appear unable to explain the isotopic, moderately volatile as well as major element composition, and geophysics of Mars simultaneously, because at least one of these properties cannot be matched. In view of the fact that many models discussed in Fig. 1 relied on limited or partly outdated data, it seems pertinent to explore the question of whether or not internally self-consistent meteorite mixing models can be formulated using the most up-to-date isotopic, geochemical, and geophysical data.

5.2. *Monte Carlo model results*

To do so, we created ten million random mixtures and tested each of these against the observed isotopic signature of Mars (Table 4) using different sets of isotopes (Table 5). In a first simulation (filter set 1, FS1), all isotopic constraints listed in Table 4 were applied, resulting in zero matches. Similarly, we obtained no matches in a second simulation (filter set 2, FS2), where Δ^{17}O was omitted. In a third simulation (FS3), we considered only the lithophile elements (O, Ca, Ti, Sr, Zr), whose isotopic signals in the Martian mantle are unaffected by core formation and therefore representative of its accretion history. This simulation resulted in 2245 successful matches. Extending the set of lithophile elements to include the weakly-siderophile Cr decreases the number of successful solutions to 833 (FS4).

In the following we focus on the solutions of FS3, since FS4 shares the same characteristics with FS3 but with fewer matches, and perform principal component analysis (PCA) as a means of grouping the solutions into clusters. From this, we obtain four distinct clusters, which are dominated by mixtures of $\gtrsim$80% O and E chondrites (Fig. 2). Two clusters mainly consist of H+EL and H+EH with varying proportions of the two components ranging from about 20% H and ∼70% EL/EH to about 50% H and 40% EL/EH. The other two clusters are principally composed of LL+EL or L+EH. The maximum amount of CC is limited to 9%, achondrites (AC) do not exceed 20% in any of the mixtures, and APB is present with a maximum of 18%. However, the majority of solutions are entirely dominated by EC and OC with very limited amounts of either CC or AC, or both (Fig. 2b). For example, more than 90% of the solutions contain less than 10% CC plus AC. The overall distribution of solutions in PCA space closely resembles results for the “chondrite-only” model of Liebske and Khan (2019) (cf. their Fig. 2a). However, because the amount of APB+EPB in the current set of models is comparably low, no additional clusters with significant AC components are present ($\leq$20% here vs. up to 71% in the achondrite model of Liebske and Khan, 2019, see their Fig. 5). The reason for the reduction in matching solutions and number of clusters relative to Liebske and Khan (2019), is a direct consequence of the much tighter present-day isotopic constraints, relative to what was available in 2019. For example, where Liebske and Khan (2019) employed a value of -0.11 ± 0.72 for ϵ^{48}Ca for Mars, the present value is -0.2 ± 0.02, which represents a considerable improvement from an observational point of view (Table 4).

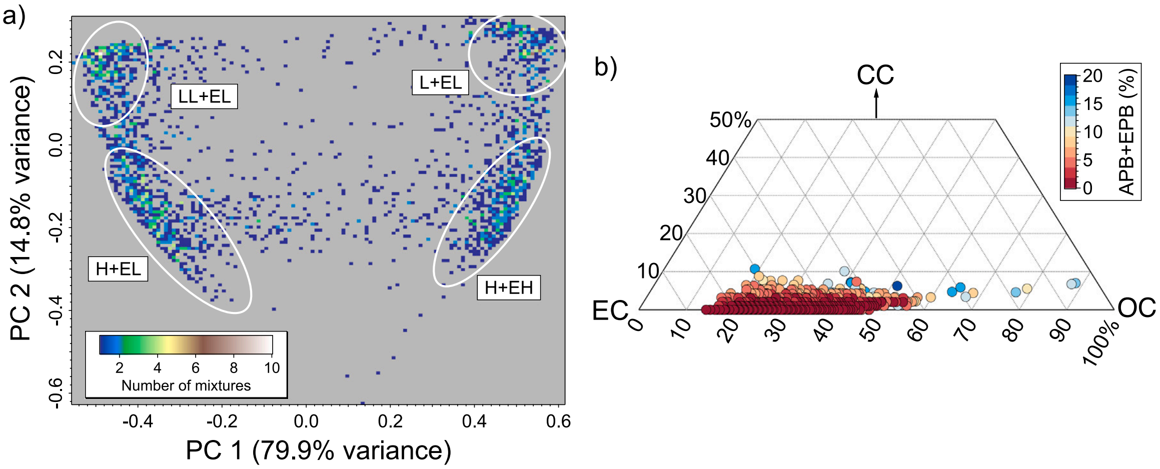

Fig. 2. Cluster analysis of random mixtures of meteoritic endmembers matching the measured isotopic anomalies for Mars (FS3, Table 5). (a) Principal component analysis (PCA) indicates four clusters of mixtures, dominated by ordinary (H, L, LL) and enstatite (EH, EL) chondrites. (b) Representation of mixtures as ternary diagram with carbonaceous- (CC), enstatite (EC)- and ordinary (OC) chondrite groups located at the apexes. Projected from achondrites (APB+EPB), whose percentages are imposed as colour. Note that most solutions fall near the EC-OC baseline. (For interpretation of colors the reader is referred to the web version of this article).

By analogy with Fig. 1, we summarise the isotopic, moderately volatile, and major element composition as well as geophysical predictions of the FS3 mixtures in Fig. 3 , from which we make the following observations:

- Instead of plotting Ti and Cr isotopes as done in Fig. 1, we show the solutions of FS3 in terms of μ^{84}Sr vs. Δ^{95}Mo in order to compare a lithophile element (Sr, filtered to fit Mars) and a siderophile element (Mo, not constrained to fit Mars) to elucidate the potential for accretion of heterogeneous components to Mars (Fig. 3a). The choice for plotting these anomalies is to highlight two key points. Firstly, the μ^{84}Sr value of Mars only partly overlaps within error with OCs, ECs and ACs, which could either indicate that Mars is an endmember with respect to Sr isotopes or, more likely, the currently-available data are insufficient for rigorous conclusions as only two Martian meteorites were measured so far for Sr, both from the same study (Moynier et al., 2012). If using the OC and EC data from Moynier et al. (2012) so as to ensure internal consistency with the Martian estimate, then all three isotopic reservoirs are within uncertainty of one another. Secondly, while no solutions exist that match Δ^{95}Mo (c.f. FS1 and FS2), some mixtures of FS3 nevertheless satisfy constraints from the other siderophile anomalies ϵ^{92}Mo, ϵ^{64}Ni and ϵ^{54}Cr, (although not simultaneously) even though these were not included as filter criteria (see Appendix B, Fig. B.1). The match to Δ^{95}Mo could potentially be improved through addition of carbonaceous material at a late stage in the accretion of Mars (e.g., Dauphas, 2017; Dauphas et al., 2024). Given that the Mo/Sr of the proto-Martian (pM) mantle should be lower than that of CI chondrites, since Mo is more siderophile than Sr, we show that for ratios of $(\mathrm{Mo/Sr})_{\mathrm{pM}}$ to $(\mathrm{Mo/Sr})_{\mathrm{CI}}$ below ~0.5, would pass through the blue field in Fig. 3a with ~10 wt % CI chondrites required. Correspondingly lower ratios of $(\mathrm{Mo/Sr})_{\mathrm{pM}}$ to $(\mathrm{Mo/Sr})_{\mathrm{CI}}$ imply lower CI mass fractions (e.g., for a ratio of 0.1, 2.5 wt % CI is required).
- Based on the solutions shown in Fig. 3b, however, the Monte Carlo mixing models in FS3 have elevated K/Th and lower Mg/Si ratio with respect to observations. Indeed, small additions of CI material (as described above in point 1) do not ameliorate this mismatch. Instead, significant amounts of e.g., APB (see Fig. 1b) would be required for these compositional constraints to be satisfied. The same principle can be observed when additionally applying Al/Si as major element constraints (Fig. 3c), where the solutions that are dominated by OC and EC, show a significant mismatch towards lower values in both Mg/Si and Al/Si, which again could be compensated for by the addition of APB or CV, however, this is in contradiction with the current isotopic data.
- The predicted geophysical responses are shown in Fig. 3d and indicate that the majority of mixtures composed of H and EL/EH chondrites (c.f. Fig. 2a) have too high mean densities and/or too low MoIs. However, two solutions nearly match mean density and MoI of Mars within uncertainties (objects labelled A and B in Fig. 3d). Mixture A is predominantly composed of H-chondrites (72%), APB (10%) and minor amounts of other components, whereas object B consists primarily of OC (55%), EC (25%) and APB (15%) (see Table C.1 for details). Object A is the closest to the Martian target range and although it nearly matches Mg/Si, it is inconsistent with the observed K/Th ratio. For an object to match mean density and MoI requires changes to mantle and core properties as demonstrated earlier (e.g., Khan et al., 2018; Liebske and Khan, 2019). We therefore modified object A through geophysical optimisation (for details see Appendix C) by changing compositional and thermal parameters of mantle and core (Table A.1). The resultant composition and core mass fraction is summarised in Table C.2.

Lastly, in two final simulations we further omitted μ^{84}Sr and Δ^{95}Mo (FS5) and μ^{84}Sr, Δ^{95}Mo, and Δ^{17}O (FS6), respectively, for which 882 solutions (FS5) and 6716 (FS6) solutions were obtained. These solutions again illustrate that, in particular Δ^{95}Mo, severely restricts the number of successful mixtures, interestingly not so ϵ^{92}Mo (see discussion on the fidelity of Δ^{95}Mo-derived estimates, below). Overall, the solution space is similar to FS3, i.e., dominated by OC and EC, with no additional apparent distinct mixing clusters. On the other hand, relaxing the isotopic constraints as done for FS5 and FS6 allows ~1/3 more CC and AC material to be mixed in (max. 12 vs. 9% CC, 34% vs. 20% AC for FS6 vs. FS3, respectively), which results in additional solutions that fall somewhat closer to the target values in K/Th vs. Mg/Si space. In any case, K/Th values for FS3 and FS6 remain too high by a factor of ~2–3.

Thus, as with Fig. 1, the conclusion that the current set of meteorites is unable to match Mars's isotopic, moderately volatile, and major element composition, along with geophysics, appears inescapable.

6. Discussion

6.1. Comparison with isotope mixing models

Each of the most recently proposed provenance models that consider multiple isotope systems for constraining endmember proportions

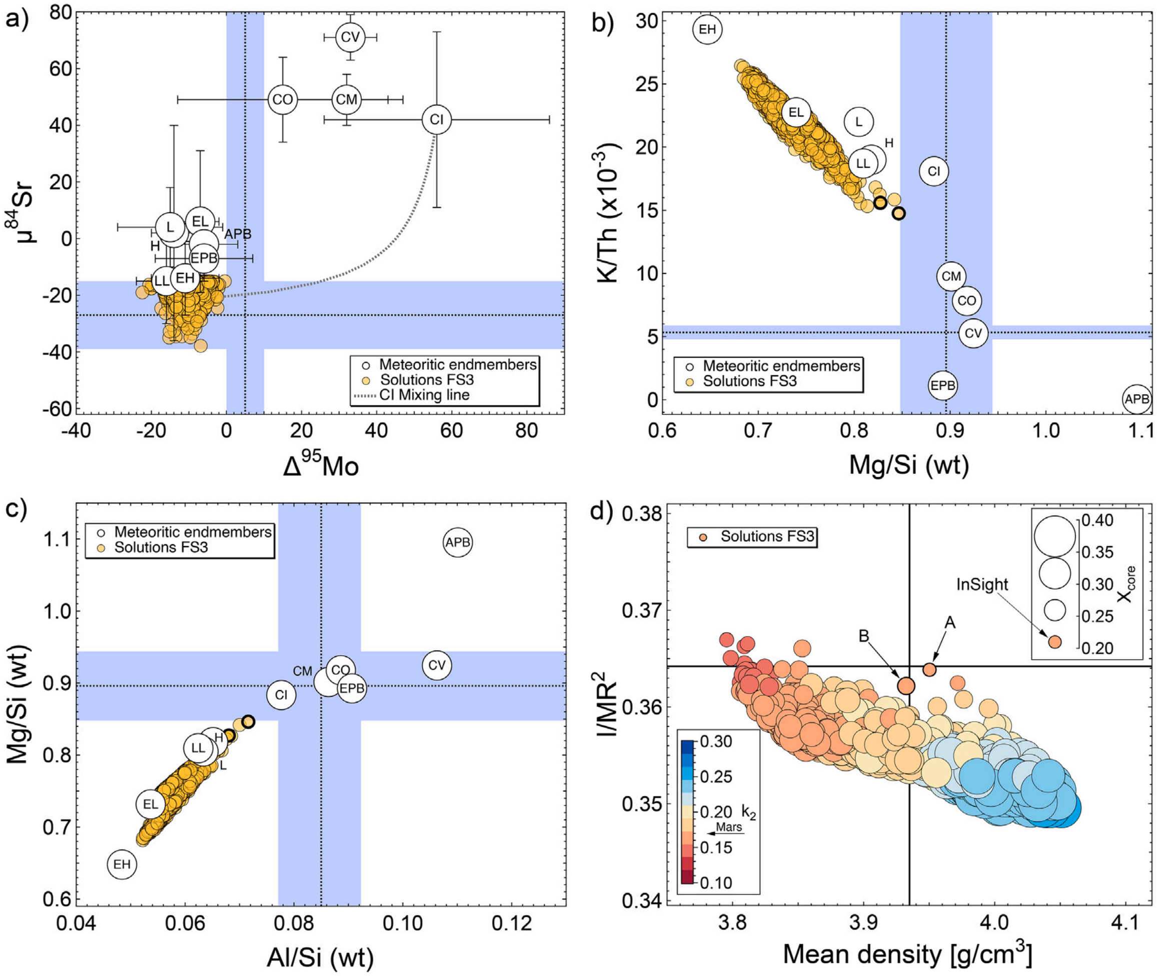

Fig. 3. Distribution of random mixture solutions (FS3) in isotopic, geochemical and geophysical space. Comparison of predictions based on FS3 and meteoritic endmembers against observations, illustrated with nucleosynthetic isotope anomalies of (a) Sr vs. Mo; (b) and (c) moderately volatile (K/Th) and major (Mg/Si, Al/Si) element ratios, respectively, and (d) geophysical properties in the form of mean moment of inertia (I/MR^2) vs. mean density. The encircled points labelled A and B indicate two solutions that are relatively close to the Martian geophysical observations. In panels (b) and (c) points A and B are indicated by thicker strokes, where A is the point located closest to the target range. Horizontal and vertical lines and blue bars indicate observed Martian values and uncertainties, respectively. "InSight" refers to the recent seismic determination of core mass fraction (Table 3). (For interpretation of colors the reader is referred to the web version of this article).

encounters difficulties when all of the constraints proposed in this study are combined. When compared to other studies including achondritic material (APB and EPB, e.g., Fitoussi et al., 2016; Liebske and Khan, 2019), we find significantly lower proportions of potential differentiated building block material (<20%) as a consequence of the improved isotopic averages for the various meteorite classes that have become available over recent years. A potential exception is model D2 of Dauphas et al. (2024) (c.f. Table 1, ~39% APB), which relies on statistically-modified isotopic values (see further discussion below). However, model D2 is nearly a factor of two too high in K/Th and lies beyond the required geophysical ranges (Fig. 1d). Models that do not consider APB or EPB, such as D1 from Dauphas et al. (2024), and the one of Brasser et al. (2018), on the other hand, are part of the FS3 solution space (see Table 1 vs. Fig. 2b), indicating some general convergence in isotope mixing models independent of the applied methodology.

Unlike the other isotope ratios, the Δ^{95}Mo denomination is defined relative to the linear relationship expressed by non-carbonaceous meteorites in ϵ^{94}Mo-ϵ^{95}Mo space (Budde et al., 2019), that is, Δ^{95}Mo = (ϵ^{95}Mo-0.596·ϵ^{94}Mo)×100. It is therefore associated with a larger uncertainty than most other isotopic ratios considered here. We further note that ϵ^{94}Mo, used in the calculation of Δ^{95}Mo, was recently shown to vary with the mass-dependent isotopic composition, δ^{98}Mo, preserved in the same samples (Budde et al., 2023; Bermingham et al., 2024), such that placing too much weight on variations in Δ^{95}Mo to provide unequivocal constraints on the provenance of Mars should be treated with caution. Another caveat pertains to the lack of ϵ^{100}Ru isotopic data for Martian meteorites. The inclusion of Ru would extend the range of elements with siderophile character treated in this work, and would provide insight into the nature of late-accreting material (or lack thereof).

It is worth noting that Dauphas et al. (2024) recognised that isotope mixing models are inconsistent with major element geochemistry but nevertheless chose to only consider the isotopic constraints. In doing so, they appealed to “hypothetical building blocks” based on the major meteorite groups but whose isotopic compositions are not derived simply from analytical measurements, but rather from statistically transformed values obtained through Bayesian inference analysis, in which the actual measurements made on meteorites are used as priors. This raises a philosophical question of whether such an approach actually evaluates the building blocks of Mars (and Earth), or rather some hypothetical planet(s) with similar isotopic compositions, to the degree that the calculated “hypothetical building blocks” were actual objects in the early solar system, but with different geochemical and geophysical characteristics.

6.2. Compositional effects on geophysical properties

As demonstrated in Fig. 3, mixtures of known types of chondrites and achondrites are able to reproduce a Mars-like signature isotopically, yet fail to reproduce the geophysical constraints. The question arises as to what controls the particular trends seen in Fig. 3d. To address this, we explore how planet compositional variations affect bulk geophysical properties. As a starting point we consider an arbitrary model planet that has properties similar to those of H-chondrites and systematically vary mantle and core chemistry, and/or mass fractions to investigate their effects on geophysical properties. The results are shown in Fig. 4 and the point where the coloured curves intersect represents the properties of the model planet that acts as reference for compositional variations.

The various models in Fig. 4 show trends from being near-vertical to near-horizontal in I/MR^2–$\bar{\rho}$ (mean normalised MoI versus mean planet density) space, although the two parameters are always negatively correlated. More specifically, we can make the following observations:

- The almost vertical trend (purple points) represents a model in which the total Fe content (Fe^{total}) is kept constant, but is partitioned between FeO in the mantle and as Fe metal in the core, for a fixed S fraction (X_S) of 0.1. The mantle and core composition, and their mass fractions, change as a consequence. While I/MR^2 shows large variations, mean planet density is nearly constant because the total iron content remains fixed.
- To conceptually simulate the effect of core oxidation (or mantle FeO reduction, blue points), we again fix Fe^{total} and Fe^{total}/Si, and vary simultaneously Fe in the core and FeO in the mantle. This also causes X_S to change because the absolute amount of S in the core is considered constant. The model that comes closest to I/MR^2 and the Martian planet density has a total Fe content of 27.5 wt%, an FeO mantle concentration of ~16.5 wt%, and a core mass fraction (X_{core}) of 0.19 with 10 wt% S.
- Near-horizontal trends are obtained when only mantle composition is changed, while keeping both X_S and X_{core} constant, as illustrated with the dark green (variations in Mg#) and light green points (Mg/Si) points, respectively.
- Diagonal trends, on the other hand, occur when core size or composition is changed for a fixed mantle composition. Illustrated here are the cases, where X_{core} is kept constant while varying X_S (orange points) and where core and mantle composition are fixed, but core mass and hence total Fe content are systematically modified (red points). We should note that in the former case X_S may be regarded as proxy for all possible light elements. Although this represents a simplification, it suffices for the purpose of studying variations in core density, as it is irrelevant by which elements this is caused, unless their individual effects were to be quantified. Both scenarios display the same general trend that is expected for planets with, relative to Mars, less massive or smaller cores. These cases are generally located in the upper left-hand quadrant. Objects with comparably larger cores instead plot towards the lower right-hand corner. Differences are also apparent in the slopes of the two model cases, more so for planets with large dense cores, as indicated in the lower right quadrant.

As mentioned, all scenarios considered in Fig. 4 show a negative correlation between MoI and mean planet density to different degrees, but the effect on both parameters is most pronounced when changing core size or composition. The most likely processes by which physical properties for endmember mixtures can be altered are through redox reactions involving the volatile species H_2O and C, or by core-mantle partitioning of potential light elements, such as H, O, and C, during accretion as explained in Section 4.2. The latter scenario is also consistent with low-density constraints for the Martian core that require the presence of elements other than sulfur (e.g., Khan et al., 2022; Huang et al., 2023). If true, this implies that mixtures located south-east relative to Martian values may evolve towards those under appropriate core formation conditions. However, from the four OC–EC dominated clusters of FS3, only mixtures rich in H+EH, and possibly EH+L (see Fig. 3d), are feasible candidates to converge to Martian values by dissolution of light elements into core liquids. Similarly, oxidation of core material (i.e. by reaction (3)) provides another possibility to render some H-chondrite-rich mixtures geophysically compatible by increasing I/MR^2 for appropriate mean densities, while reduction of FeO through C (reaction (4)) would increase the mismatch with Martian values.

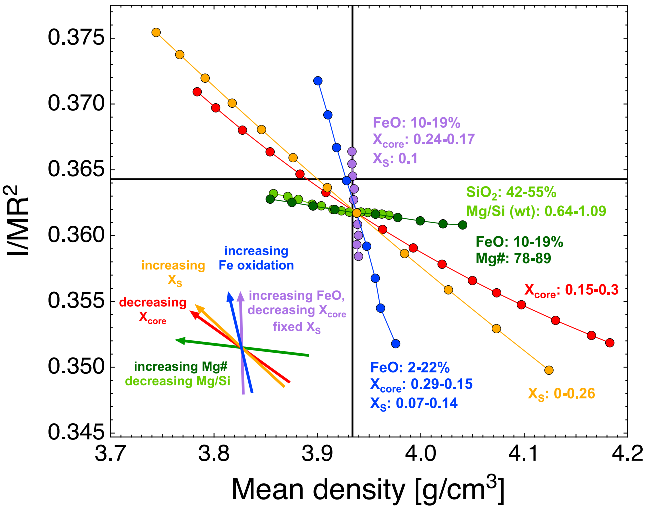

Fig. 4. Compositional trends and geophysical response. The coloured lines and points indicate the variation in mean density vs. mean moment of inertia (I/MR^2) as a function of changes in mantle composition (MgO, SiO_2, FeO), core composition (sulfur content, X_S) and size (core mass fraction, X_{core}). The parameters that are being varied are indicated in the coloured text next to or below each line. Arrows at the bottom left indicate the general direction of geophysical change as a function of parameter variation. The central point where all models cross has properties similar to a pure H chondrite with a core- and sulfur- mass fraction of X_{core} = 0.21 and X_S = 0.1, respectively, a mantle Mg# (molar Mg/(Mg+Fe)×100) of 80.5, and a mantle Mg/Si weight ratio of 0.69. Black horizontal and vertical lines represent Martian values. (For interpretation of colors the reader is referred to the web version of this article).

6.3. Comparison with predictions from planetary accretion models

There are two major models for the accretion of the terrestrial planets (including Mars): the classical planetesimal hypothesis (Wetherill, 1980) and the more recently developed pebble accretion hypothesis (Lambrechts and Johansen, 2012). The pebble accretion model (see also Morbidelli et al., 2025; Bizzarro et al., 2025, for recent reviews), whereby the planets grow by the accumulation of relatively small (mm-to-cm scale) bodies, was developed largely to explain the formation of the giant planets (especially their large cores) but also has important implications for the formation of the terrestrial planets (Levison et al., 2015). Among the key predictions of the pebble accretion model, as presently conceived, are that the amount of outer solar system material (i.e., carbonaceous chondrites) that was accreted to form terrestrial planets was relatively large as compared to the requirements of the planetesimal hypothesis (Johansen et al., 2021) and the relative proportions of CC may have increased as accretion proceeded (Schiller et al., 2018). A number of workers (e.g., Mah et al., 2022; Morbidelli et al., 2025) have pointed out that the isotopic data may limit the amount of CC to levels insufficient to be consistent with pebble accretion being

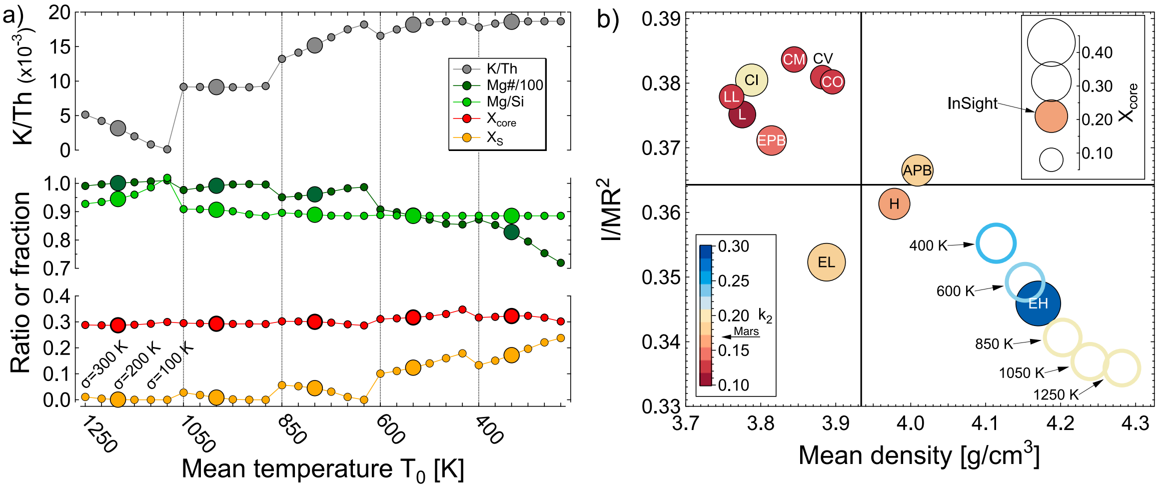

Fig. 5. Geochemical and geophysical properties of solar nebular condensates. (a) Geochemical parameters in the form of K/Th, Mg#, Mg/Si, core mass fraction (X_{core}) and sulfur content (X_S) of condensed compositions formed at mean temperatures (T_0) from 1250 K to 400 K. For each T_0, results for five different standard deviations (σ; 300, 250, 200, 150, 100 and 50 K; see text for details), are plotted from left to right as circles. The large circles represent σ = 200 K for which geophysical properties are shown in panel (b). Note that Th was calculated from the concentrations of Al and assuming a CI-chondritic Al/Th ratio. (b) Computed geophysical properties of condensates (σ = 200 K, open coloured circles) and meteoritic endmembers. The observed trend towards lower mean density and higher I/MR^2 is mainly caused by increasing core sulfur content (X_S) and oxidation of Fe to FeO with decreasing T_0, particularly for T_0 ≤600 K. (For interpretation of colors the reader is referred to the web version of this article).

dominant for the growth of the terrestrial planets. Our findings appear to be fully consistent with such a conclusion, as all of our mixing models limit the amount of CC material in Mars to less than about 9%, and ~98% of the mixtures contain less than 5% (Fig. 2b). We therefore conclude that, were the importance of pebble accretion to be equated with the CC fraction of Mars, then it could not have been a volumetrically significant process governing its accretion. On the other hand, if 'non-carbonaceous (NC)-like' pebbles existed, our results would not exclude the role of pebble accretion from a physical standpoint. That is, pebble accretion may still be a viable physical process in forming Mars, provided such pebbles had NC-like characteristics (i.e., H_2O-poor and originated in the inner solar system).

6.4. What is Mars made of?

Our analysis clearly establishes that the known collection of meteorites does not include at least one of the dominant building blocks that form Mars. The obvious question then is what is the nature of that component (or components)? Although there is considerable uncertainty in quantifying exact mixing matches, the isotopic data provide compelling evidence that such material is most likely intrinsic to the inner solar system (i.e., NC-like with respect to isotopes to more than 90–95 %; Figs. 2b, Fig. 3a). However, as demonstrated above, in terms of major elements (e.g., Mg/Si, Al/Si) the material appears most similar to carbonaceous chondrites CI, CM, and CO or possibly differentiated bodies of the NC group, such as 4-Vesta (i.e. EPB, Fig. 1c) and the volatile elements further constrain such material to be most similar to CV or mixtures between carbonaceous chondrites and a differentiated body such as EPB or APB (Fig. 1b). The CV group also simultaneously accounts for the combined Mg/Si and K/Th ratios inferred for bulk Mars. However, such an agreement may be fortuitous, as any volatile-rich NC body (e.g., EH) and a volatile-poor NC object (e.g., the APB) could be mixed together in proportions so as to yield Mars-like Mg/Si and K/Th ratios. In general, however, the broad similarity between moderately volatile element depletion patterns in the Earth and Mars and those found in CV or CO chondrites has been noted previously (Witt-Eickschen et al., 2009; Braukmüller et al., 2019; Mezger et al., 2020), yet, in detail, differences exist that do not require a CC-like mode of volatile depletion for either planet (Khan et al., 2022; Sossi et al., 2022).

On the basis of existing bodies sampled in the meteorite collection, there is little- to no systematic difference in the abundances of the moderately volatile elements between CC and NC groups (cf. Table 2). The key distinction arises among the true volatile (so-called 'ice-forming') elements, notably C and H. Sulfur, belonging to the moderately volatile group of elements, is similarly abundant in EH and CI chondrites, an observation that holds for other moderately volatile elements, such as Zn or K (see Table 2 for K). Therefore, insofar as there is no evidence that Mars is anomalously rich in H or C compared to other NC bodies, then there is no requirement that it accreted from any significant fraction of outer solar system (CC) material. Indeed, the main 'light' constituent of the Martian core is S (Huang et al., 2023; Khan et al., 2023), a property entirely consistent with its proposed origin as an NC body.

Finally the geophysics is best explained if the accreting material is relatively oxidised. Most isotopic mixing solutions determined in this study indicate a moment of inertia that is too low for the known density (Fig. 3d); that is, the core mass fraction derived from a mixture of ordinary- and enstatite chondrites (required to fit the isotopic data) is too high (~0.3) relative to that observed of Mars (0.21; Khan et al., 2023). The most efficient way to increase the moment of inertia without significantly changing density is to simply oxidise metal to form FeO in the mantle (blue trend in Fig. 4). This could be achieved in two ways; (i) core Fe-oxidation at constant bulk composition if reaction (5) proceeds from the right- to the left-hand side, a process not considered in our model, or (ii) addition of O to the bulk compositions of chondrites. Option (i) can be excluded owing to the high FeO content of the Martian mantle (Khan et al., 2022) and the relatively shallow core-mantle boundary on Mars; the implication being that the temperatures of core formation, if constrained to lie on a magma ocean adiabat, would have been too low to induce significant Si dissolution (Gessmann et al., 2001; Fischer et al., 2015; Huang et al., 2019).

In order to test option *(ii)*, we perform simulations of nebular condensation of the solar composition (Lodders, 2023) at equilibrium at a constant pressure and 10 K intervals from 1700 to 300 K (10^{-4} bar) using FactSage 8.2 (Bale et al., 2016). We considered the major elements, H, He, C, N, O, Si, Mg, Fe, Ni, Al, Ca, Ti, Cr, Mn, S, Na and K in our analysis, and used solid solution models, where stable, in the FT-misc and FToxid databases of FactSage, in addition the standard FactPS database that contains pure condensed phases and gas species. The resulting sequence of condensed phases were then 'mixed' by assuming that Mars could have formed from a Gaussian distribution of such condensates, which have been shown to match the bulk composition of the Earth (Sossi et al., 2022). In order to do so, we follow the approach of Sossi et al. (2022), in which the mean temperature of the distribution, T_0, and its standard deviation, σ, are varied systematically between 400 K and 1250 K (T_0) and between 50 K and 300 K (σ) at each T_0, respectively. Converting these bulk compositions (chemical characteristics shown in Fig. 5a) into mantle- and core compositions by the same procedure as outlined for other materials (Section 4.2), and applying the subsequent geophysical treatment to compute MoI and mean density (Section 4.3), the results show that such mixtures occupy the lower right-hand quadrant relative to Mars (Fig. 5b). That is, these compositions are too reduced (i.e., the FeO/Fe ratio is too low), leading to moments of inertia that are too low and mean densities that are too high with respect to those of Mars. Even though condensates evolve towards Mars-like moments of inertia with decreasing T_0 they still have too high mean densities, and importantly, at 400 K the abundance of moderately volatile elements (K/Th and X_S) is far too high as illustrated in Fig. 5a with respect to the observed quantities in Mars (which are consistent with T_0 ~1100 K, see Khan et al., 2022). This exercise confirms the notion that the volatile-depleted nature of Mars' building blocks (relative to chondrites) must be coupled with a relatively high FeO/Fe ratio, two traits that are not readily observed together in planetary materials; neither among chondrites nor in mixtures of equilibrium condensates of the solar nebula.

To summarise, the simplest way to explain these disparate isotopic, geochemical and geophysical observations is to suggest that the "missing" building blocks from which Mars is made appear to be bodies that are intrinsic to the inner solar system but that are relatively oxidised and have been influenced by evaporation/condensation processes that lead to the significant volatile-element depletion under conditions that were likely distinct from those of existing meteorites.

7. Conclusions

In this study we sought to constrain the nature and provenance of the material from which Mars accreted. In view of the fact that several published bulk chemical models of Mars are unable to simultaneously explain its isotopic, moderately volatile, and major element composition and geophysical properties, we explored whether internally self-consistent meteorite mixing models can be formulated using the most up-to-date isotopic, geochemical, and geophysical data. For this, we have built upon and extended the work of Liebske and Khan (2019) by including a plethora of data that pertain to the constitution and origin of Mars, including higher-quality isotopic measurements of Martian meteorites, refined chemical compositions of meteoritic end-members, and, not least, results from the InSight mission that provided the first direct constraints on the interior structure of Mars. Based on the integration of these data sets, which is what allows us to go beyond otherwise non-unique meteoritic mixing models when viewed in isotopic space alone, we find that

- from an isotopic standpoint, Mars consists primarily of ordinary and enstatite chondrites, while achondritic and carbonaceous chondritic material play subordinate roles. Such mixtures, however, are unable to match the moderately volatile, major element and geophysical characteristics of Mars;
- from a geophysical point of view, the angrite parent body (APB) has similar properties to Mars and can act as a complement to OC/EC-based mixtures to compensate for their low Mg/Si and Al/Si and too high K/Th ratios. Relying on the current database of measured isotopic data, the contribution of APB to any mixture, however, cannot exceed ~20%;
- the inability to self-consistently account for all observations suggests that Mars possibly formed from meteoritic material that is either no longer extant or as yet remains unsampled;
- our analysis, instead, seems to indicate that relatively oxidised material, inherent to the inner solar system and that has undergone evaporation/condensation processes leading to volatile-element depletion patterns, which, in detail do not replicate those in any known meteorite group, would be consistent with the isotopic, geochemical and geophysical properties of Mars.

Table A.1
Summary of model parameters used for computing geophysical properties and observations. Crust and mantle composition rely on the NCFMAS model chemical system, comprising the oxides of Na_2O-CaO-FeO-MgO-Al_2O_3-SiO_2. Prior ranges are taken from Khan et al. (2023), whereas crustal thickness is based on the average value from Kim et al. (2023). Parameters C_{mantle}, X_S, and R_{core} are subject to the core-mantle mass exchange reaction (Section 4.2) and therefore not independently variable.

Parameter	Description	Value	Prior range
d_{moho} (km)	Crustal thickness	50	Fixed
T_{surf} (K)	Surface temperature	173	Fixed
T_{lit} (K)	Base lithosphere temperature	1800	1700–1900
d_{lit} (km)	Lithospheric thickness	425	400–500
C_{crust} (wt%)	Crustal composition	Taylor and McLennan (2009)	Fixed
C_{mantle} (wt%)	Mantle composition	Mass balance	Variable
X_S (wt%)	Core composition (S content)	Mass balance	Variable
R_{core} (km)	Core radius	Mass balance	variable

CRediT authorship contribution statement

Christian Liebske: Writing – review & editing, Writing – original draft, Methodology, Investigation, Conceptualization. **Amir Khan:** Writing – review & editing, Writing – original draft, Methodology, Investigation, Funding acquisition, Conceptualization. **Scott M. McLennan:** Writing – review & editing, Writing – original draft, Methodology, Investigation, Funding acquisition, Conceptualization. **Paolo A. Sossi:** Writing – review & editing, Writing – original draft, Methodology, Investigation, Funding acquisition, Conceptualization.

Declaration of competing interest

The authors declare that they have no known competing financial interests or personal relationships that could have appeared to influence the work reported in this paper.

Acknowledgements

We are grateful to Debarun Mukherjee and an anonymous referee for thorough reviews that helped improve the clarity of the manuscript considerably. We would also like to thank A. Morbidelli for efficient editorial handling. We acknowledge support from the Swiss National Science Foundation for a visiting grant to S.M.M. (project 225202). P.A.S. is grateful to the Swiss National Science Foundation via an Eccellenza Professorship (203668) and the Swiss State Secretariat for Education, Research and Innovation (SERI) under contract number MB22.00033, a SERI-funded ERC Starting Grant "2ATMO". Finally, as all authors have contributed equally to this study, author order was decided by random draw.

Appendix A. Geophysical parameters

See Table A.1.

Appendix B. Isotopic signatures of siderophiles for FS3

Although FS3 was filtered for a lithophile element signature, a number of mixing solutions fulfil constraints for ϵ^{92}Mo (1307 matches), ϵ^{64}Ni (585 matches), and the weakly siderophile ϵ^{54}Cr (764 matches, i.e., similar to FS4). As an illustration hereof, we show the distribution of ϵ^{54}Cr vs. ϵ^{92}Mo for FS3.

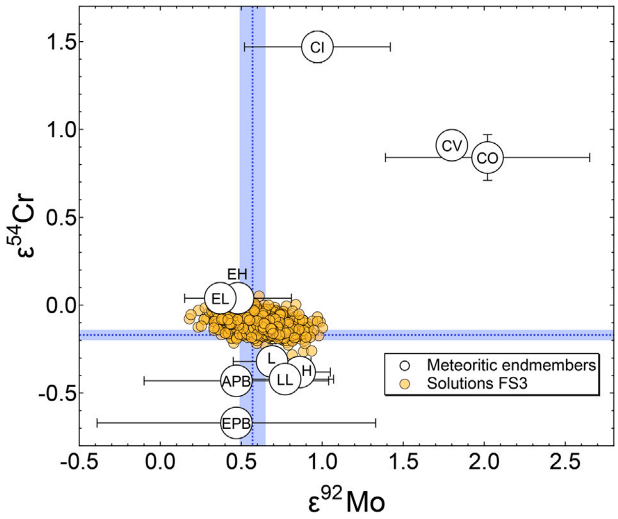

Fig. B.1. FS3 solutions for Cr and Mo isotopic compositions. Note that CM, for which ϵ^{92}Mo = 5.7, is not shown. For Mo data points spread nearly symmetrically around the Martian target, whereas they are offset towards EC for Cr. Horizontal and vertical lines and blue bars indicate observed Martian values and uncertainties, respectively.

Appendix C. Geophysical optimisation

Here we briefly describe how the bulk compositional models are optimised to match the Martian geophysical observations. The optimisation problem, which is formulated as an inverse problem, can formally be written as $\mathbf{d} = g(\mathbf{m})$, where $\mathbf{d}$ is a data vector consisting of observations and g is a forward operator that enables us to compute geophysical data for a given model $\mathbf{m}$. To solve the inverse problem, we employ a Bayesian approach (Mosegaard and Tarantola, 1995), which combines prior information on model parameters with information from data and physical models

$$\sigma(\mathbf{m}) = k f(\mathbf{m})\mathcal{L}(\mathbf{m}), \tag{C.1}$$

where k is a normalisation constant, $f(\mathbf{m})$ is the prior model parameter probability distribution, $\mathcal{L}(\mathbf{m})$ is the likelihood function, and $\sigma(\mathbf{m})$ is the posterior model parameter distribution. Prior information (Table A.1) represents information on model parameters obtained independently of data and the likelihood function measures the misfit between observed and predicted data. Assuming that data noise is Gaussian distributed and that observational uncertainties and calculation errors are independent among the data, the likelihood function can be written as

$$\mathcal{L}(\mathbf{m}) \propto \prod_{\mathrm{i}} \exp\left(-\frac{|\mathrm{d}^{\mathrm{i}}_{\mathrm{obs}} - \mathrm{d}^{\mathrm{i}}_{\mathrm{cal}}(\mathbf{m})|^2}{2\sigma_{\mathrm{i}}^2}\right) \tag{C.2}$$

where i runs over $\bar{\rho}$, I/MR^2, and k_2, $\mathrm{d}_{\mathrm{obs}}$ and $\mathrm{d}_{\mathrm{cal}}(\mathbf{m})$ denote observed and calculated data, respectively, and σ data uncertainty.

We employ a Metropolis algorithm to sample the model space of solutions to the optimisation problem. The Metropolis algorithm is an example of an importance sampling algorithm, i.e., models fitting data and consistent with prior information are sampled more frequently. In practice, the algorithm performs a "guided" random walk in the model space, where in each iteration a new proposed model, consisting of the model parameters listed in Table A.1, is sampled according to the prior distribution and the misfit of which is tested against the data through the likelihood function. In case the new proposed model results in an improved datafit, it is accepted; if this is not the case, the model may be either accepted or rejected, which is determined by the acceptance criterion (Mosegaard and Tarantola, 1995). We ran the inversion scheme for about 10^6 iterations and checked all output parameters for consistency and convergence. The optimised, i.e., best-fitting, model composition is summarised in Table C.2.

Table C.1
Mixtures of the two labelled data points in Fig. 3d used for inversion analysis.

	CI	CM	CV	CO	H	L	LL	EH	EL	APB	EPB
A	0	0	0.05	0.01	0.72	0	0.04	0.02	0.02	0.1	0.04
B	0	0.05	0	0	0.44	0	0.11	0.08	0.17	0.15	0

Table C.2
Model compositions of data point A in Figure Fig. 3d before (initial) and after (final) geophysical optimisation, respectively. Mantle oxides are in wt%, core sulfur content (X_S) and core mass (X_{core}) represent mass fractions, and Mg# the molar Mg/(Mg+Fe) ratio ×100.

	SiO_2	Al_2O_3	MgO	FeO	CaO	Na_2O	X_S	X_{core}	Mg#
Initial	45.74	3.29	29.93	17.66	2.42	0.96	0.114	0.202	75.5
Final	45.44	3.26	29.73	18.21	2.40	0.95	0.116	0.198	74.4

Data availability

All data used are reported in the manuscript.

References

Akram, W., Schönbächler, M., 2016. Zirconium isotope constraints on the composition of theia and current moon-forming theories. Earth Planet. Sci. Lett. 449, 302–310. http://dx.doi.org/10.1016/j.epsl.2016.05.022.

Anderson, D.L., 1972. Internal constitution of mars. J. Geophys. Res. 77 (5), 789–795. http://dx.doi.org/10.1029/JB077i005p00789.

Bagheri, A., Khan, A., Al-Attar, D., Crawford, O., Giardini, D., 2019. Tidal response of mars constrained from laboratory-based viscoelastic dissipation models and geophysical data. J. Geophys. Res.: Planets 124 (11), 2703–2727.

Bale, C.W., Bélisle, E., Chartrand, P., Decterov, S.A., Eriksson, G., Gheribi, A.E., Hack, K., Jung, I.-H., Kang, Y.-B., Melançon, J., et al., 2016. Factsage thermochemical software and databases, 2010–2016. Calphad 55, 1–19.

Banerdt, W.B., Smrekar, S.E., Banfield, D., Giardini, D., Golombek, M., Johnson, C.L., Lognonné, P., Spiga, A., Spohn, T., Perrin, C., Stähler, S.C., Antonangeli, D., Asmar, S., Beghein, C., Bowles, N., Bozdag, E., Chi, P., Christensen, U., Clinton, J., Collins, G.S., Daubar, I., Dehant, V., Drilleau, M., Fillingim, M., Folkner, W., Garcia, R.F., Garvin, J., Grant, J., Grott, M., Grygorczuk, J., Hudson, T., Irving, J.C.E., Kargl, G., Kawamura, T., Kedar, S., King, S., Knapmeyer-Endrun, B., Knapmeyer, M., Lemmon, M., Lorenz, R., Maki, J.N., Margerin, L., McLennan, S.M., Michaut, C., Mimoun, D., Mittelholz, A., Mocquet, A., Morgan, P., Mueller, N.T., Murdoch, N., Nagihara, S., Newman, C., Nimmo, F., Panning, M., Pike, W.T., Plesa, A.-C., Rodriguez, S., Rodriguez-Manfredi, J.A., Russell, C.T., Schmerr, N., Siegler, M., Stanley, S., Stutzmann, E., Teanby, N., Tromp, J., van Driel, M., Warner, N., Weber, R., Wieczorek, M., 2020. Initial results from the InSight mission on mars. Nat. Geosci. 13 (3), 183–189. http://dx.doi.org/10.1038/s41561-020-0544-y.

Bermingham, K.R., Tornabene, H.A., Walker, R.J., Godfrey, L.V., Meyer, B.S., Piccoli, P., Mojzsis, S., 2024. The non-carbonaceous nature of earth's late-stage accretion. Geochim. Cosmochim. Acta.

Bermingham, K., Worsham, E., Walker, R., 2018. New insights into mo and ru isotope variation in the nebula and terrestrial planet accretionary genetics. Earth Planet. Sci. Lett. 487, 221–229.

Bertka, C.M., Fei, Y., 1998. Density profile of an SNC model martian interior and the moment-of-inertia factor of mars. Earth Planet. Sci. Lett. 157, 79–88. http://dx.doi.org/10.1016/S0012-821X(98)00030-2.

Binder, A.B., 1969. Internal structure of mars. J. Geophys. Res. 74, 3110–3118. http://dx.doi.org/10.1029/JB074i012p03110.

Bizzarro, M., Johansen, A., Dorn, C., 2025. The cosmochemistry of planetary systems. Nat. Rev. Chem. 1–19.

Bouvier, A., Boyet, M., 2016. Primitive solar system materials and earth share a common initial 142Nd abundance. Nature 537 (7620), 399–402.

Brasser, R., Dauphas, N., Mojzsis, S.J., 2018. Jupiter's influence on the building blocks of mars and earth. Geophys. Res. Lett. 45 (12), 5908–5917. http://dx.doi.org/10.1029/2018GL078011.

Brasser, R., Mojzsis, S., Matsumura, S., Ida, S., 2017. The cool and distant formation of mars. Earth Planet. Sci. Lett. 468, 85–93. http://dx.doi.org/10.1016/j.epsl.2017.04.005.

Braukmüller, N., Wombacher, F., Funk, C., Münker, C., 2019. Earth's volatile element depletion pattern inherited from a carbonaceous chondrite-like source. Nat. Geosci. 12 (7), 564–568.

Brennan, M.C., Fischer, R.A., Irving, J.C., 2020. Core formation and geophysical properties of mars. Earth Planet. Sci. Lett. 530, 115923.

Budde, G., Burkhardt, C., Brennecka, G.A., Fischer-Gödde, M., Kruijer, T.S., Kleine, T., 2016. Molybdenum isotopic evidence for the origin of chondrules and a distinct genetic heritage of carbonaceous and non-carbonaceous meteorites. Earth Planet. Sci. Lett. 454, 293–303.

Budde, G., Burkhardt, C., Kleine, T., 2019. Molybdenum isotopic evidence for the late accretion of outer solar system material to earth. Nat. Astron. 3 (8), 736–741.

Budde, G., Tissot, F.L., Kleine, T., Marquez, R.T., 2023. Spurious molybdenum isotope anomalies resulting from non-exponential mass fractionation. Geochemistry 83 (3), 126007.

Burbine, T.H., O'Brien, K.M., 2004. Determining the possible building blocks of the earth and mars. Meteorit. Planet. Sci. 39, 667–681. http://dx.doi.org/10.1111/j.1945-5100.2004.tb00110.x.

Burkhardt, C., Borg, L.E., Brennecka, G.A., Shollenberger, Q.R., Dauphas, N., Kleine, T., 2016. A nucleosynthetic origin for the earth's anomalous nd-142 composition. Nat. 537 (7620), 394. http://dx.doi.org/10.1038/nature18956.

Burkhardt, C., Spitzer, F., Morbidelli, A., Budde, G., Render, J.H., Kruijer, T.S., Kleine, T., 2021. Terrestrial planet formation from lost inner solar system material. Sci. Adv. 7 (52), eabj7601.

Campbell, I.H., O'Neill, H.S.C., 2012. Evidence against a chondritic earth. Nature 483 (7391), 553–558.

Ceylan, S., Giardini, D., Clinton, J.F., Kim, D., Khan, A., Stähler, S.C., Zenhäusern, G., Lognonné, P., Banerdt, W.B., 2023. Mapping the seismicity of mars with insight. J. Geophys. Res.: Planets 128 (8), e2023JE007826. http://dx.doi.org/10.1029/2023JE007826.

Charlier, B., Tissot, F., Dauphas, N., Wilson, C., 2019. Nucleosynthetic, radiogenic and stable strontium isotopic variations in fine-and coarse-grained refractory inclusions from allende. Geochim. Cosmochim. Acta 265, 413–430.

Charnoz, S., Sossi, P.A., Lee, Y.-N., Siebert, J., Hyodo, R., Allibert, L., Pignatale, F.C., Landeau, M., Oza, A.V., Moynier, F., 2021. Tidal pull of the earth strips the proto-moon of its volatiles. Icarus 364, 114451.

Connolly, J.A.D., 2009. The geodynamic equation of state: What and how. Geochem. Geophys. Geosyst. 10 (10), Q10014. http://dx.doi.org/10.1029/2009GC002540.

Connolly, J.A.D., Khan, A., 2016. Uncertainty of mantle geophysical properties computed from phase equilibrium models. Geophys. Res. Lett. 43, 5026–5034. http://dx.doi.org/10.1002/2016GL068239.

Dauphas, N., 2017. The isotopic nature of the earth's accreting material through time. Nat. 541 (7638), 521–524. http://dx.doi.org/10.1038/nature20830.

Dauphas, N., Hopp, T., Nesvornỳ, D., 2024. Bayesian inference on the isotopic building blocks of mars and earth. Icarus 408, 115805.

Dauphas, N., Nie, N.X., Blanchard, M., Zhang, Z.J., Zeng, H., Hu, J.Y., Meheut, M., Visscher, C., Canup, R., Hopp, T., 2022. The extent, nature, and origin of k and rb depletions and isotopic fractionations in earth, the moon, and other planetary bodies. Planet. Sci. J. 3 (2), 29.

Delaney, J.S., 1994. A model composition for mars derived from the oxygen isotopic ratios of martian/SNC meteorites. Meteoritics 29 (4), 459.

Drake, M., Righter, K., 2002. Determining the composition of the earth. Nature 416 (6876), 39–44. http://dx.doi.org/10.1038/416039a.

Dreibus, G., Wänke, H., 1984. Accretion of the earth and inner planets. In: Geochemistry and Cosmochemistry. pp. 3–11.

Dreibus, G., Wänke, H., 1985. Mars, a volatile-rich planet. Meteoritics 20, 367–381.

Drilleau, M., Samuel, H., Garcia, R.F., Rivoldini, A., Perrin, C., Michaut, C., Wieczorek, M., Tauzin, B., Connolly, J.A.D., Meyer, P., Lognonné, P., Banerdt, W.B., 2022. Marsquake locations and 1-D seismic models for mars from insight data. J. Geophys. Res. (Planets) 127 (9), e07067. http://dx.doi.org/10.1029/2021JE007067.

Durán, C., Khan, A., Ceylan, S., Charalambous, C., Kim, D., Drilleau, M., Samuel, H., Giardini, D., 2022. Observation of a core-diffracted P-wave from a farside impact with implications for the lower-mantle structure of mars. Geophys. Res. Lett. 49 (21), e2022GL100887. http://dx.doi.org/10.1029/2022GL100887.

Durán, C., Khan, A., Ceylan, S., Zenhäusern, G., Stähler, S., Clinton, J.F., Giardini, D., 2022. Seismology on mars: An analysis of direct, reflected, and converted seismic body waves with implications for interior structure. Phys. Earth Planet. Inter. 325, 106851. http://dx.doi.org/10.1016/j.pepi.2022.106851.

Fischer, R.A., Nakajima, Y., Campbell, A.J., Frost, D.J., Harries, D., Langenhorst, F., Miyajima, N., Pollok, K., Rubie, D.C., 2015. High pressure metal–silicate partitioning of Ni, Co, V, Cr, Si, and O. Geochim. Cosmochim. Acta 167, 177–194.

Fischer-Gödde, M., Elfers, B.-M., Münker, C., Szilas, K., Maier, W.D., Messling, N., Morishita, T., Van Kranendonk, M., Smithies, H., 2020. Ruthenium isotope vestige of earth's pre-late-veneer mantle preserved in Archaean rocks. Nature 579 (7798), 240–244.

Fitoussi, C., Bourdon, B., Wang, X., 2016. The building blocks of earth and mars: A close genetic link. Earth Planet. Sci. Lett. 434, 151–160. http://dx.doi.org/10.1016/j.epsl.2015.11.036.

Ganapathy, R., Anders, E., 1974. Bulk composition of the moon and earth, estimated from meteorites. In: Fifth Lunar and Planetary Science Conference Proceedings. Vol. 2, pp. 1181–1206.

Gessmann, C., Wood, B., Rubie, D., Kilburn, M., 2001. Solubility of silicon in liquid metal at high pressure: implications for the composition of the earth's core. Earth Planet. Sci. Lett. 184 (2), 367–376.

Horleston, A.C., Clinton, J.F., Ceylan, S., Giardini, D., Charalambous, C., Irving, J.C.E., Lognonné, P., Stähler, S.C., Zenhäusern, G., Dahmen, N.L., Duran, C., Kawamura, T., Khan, A., Kim, D., Plasman, M., Euchner, F., Beghein, C., Beucler, É., Huang, Q., Knapmeyer, M., Knapmeyer-Endrun, B., Lekić, V., Li, J., Perrin, C., Schimmel, M., Schmerr, N.C., Stott, A.E., Stutzmann, E., Teanby, N.A., Xu, Z., Panning, M., Banerdt, W.B., 2022. The far side of mars: Two distant marsquakes detected by insight. Seism. Rec. 2 (2), 88–99. http://dx.doi.org/10.1785/0320220007.

Hu, Y., Moynier, F., Yang, X., 2023. Volatile-depletion processing of the building blocks of earth and mars as recorded by potassium isotopes. Earth Planet. Sci. Lett. 620, 118319. http://dx.doi.org/10.1016/j.epsl.2023.118319.

Huang, D., Badro, J., Brodholt, J., Li, Y., 2019. Ab initio molecular dynamics investigation of molten Fe–Si–O in earth's core. Geophys. Res. Lett. 46 (12), 6397–6405.

Huang, D., Li, Y., Khan, A., Sossi, P., Giardini, D., Murakami, M., 2023. Thermoelastic properties of liquid Fe-rich alloys under martian core conditions. Geophys. Res. Lett. 50 (6), e2022GL102271. http://dx.doi.org/10.1029/2022GL102271, e2022GL102271 2022GL102271.

Irving, J.C.E., Lekić, V., Durán, C., Drilleau, M., Kim, D., Rivoldini, A., Khan, A., Samuel, H., Antonangeli, D., Banerdt, W.B., Beghein, C., Bozdağ, E., Ceylan, S., Charalambous, C., Clinton, J., Davis, P., Garcia, R., Domenico Giardini, Horleston, A.C., Huang, Q., Hurst, K.J., Kawamura, T., King, S.D., Knapmeyer, M., Li, J., Lognonné, P., Maguire, R., Panning, M.P., Plesa, A.-C., Schimmel, M., Schmerr, N.C., Stähler, S.C., Stutzmann, E., Xu, Z., 2023. First observations of core-transiting seismic phases on mars. Proc. Natl. Acad. Sci. 120 (18), e2217090120. http://dx.doi.org/10.1073/pnas.2217090120.

Jagoutz, E., Palme, H., Baddenhausen, H., Blum, K., Cendales, M., Dreibus, G., Spettel, B., Lorenz, V., Wänke, H., 1979. The abundances of major, minor and trace elements in the earth's mantle as derived from primitive ultramafic nodules. In: Tenth Lunar and Planetary Science Conference Proceedings. Vol. 2, pp. 2031–2050.

Jarosewich, E., 1990. Chemical analysis of meteorites - a compilations of stony and iron meteorite analyses. Meteorit. 25 (4), 323–337. http://dx.doi.org/10.1111/j.1945-5100.1990.tb00717.x.

Johansen, A., Ronnet, T., Bizzarro, M., Schiller, M., Lambrechts, M., Nordlund, Å., Lammer, H., 2021. A pebble accretion model for the formation of the terrestrial planets in the solar system. Sci. Adv. 7 (8), eabc0444.

Johnston, D.H., McGetchin, T.R., Toksoez, M.N., 1974. The thermal state and internal structure of mars. J. Geophys. Res. 79, 3959–3971. http://dx.doi.org/10.1029/JB079i026p03959.

Johnston, D.H., Toksoz, M.N., 1977. Internal structure and properties of mars. Icarus 32 (1), 73–84. http://dx.doi.org/10.1016/0019-1035(77)90050-1.

Jurewicz, A., Jones, J., Mittlefehldt, D., Longhi, J., 2004. Devolatilized-allende partial melts as an analog for primitive angrite magmas. In: Lunar and Planetary Science Conference. p. 1417.

Keil, K., 2012. Angrites, a small but diverse suite of ancient, silica-undersaturated volcanic-plutonic mafic meteorites, and the history of their parent asteroid. Chem. Erde/Geochem. 72 (3), 191–218. http://dx.doi.org/10.1016/j.chemer.2012.06.002.

Khan, A., Ceylan, S., van Driel, M., Giardini, D., Lognonné, P., Samuel, H., Schmerr, N.C., Stähler, S.C., Duran, A.C., Huang, Q., Kim, D., Broquet, A., Charalambous, C., Clinton, J.F., Davis, P.M., Drilleau, M., Karakostas, F., Lekic, V., McLennan, S.M., Maguire, R.R., Michaut, C., Panning, M.P., Pike, W.T., Pinot, B., Plasman, M., Scholz, J.-R., Widmer-Schnidrig, R., Spohn, T., Smrekar, S.E., Banerdt, W.B., 2021. Upper mantle structure of mars from InSight seismic data. Science 373 (6553), 434–438. http://dx.doi.org/10.1126/science.abf2966.

Khan, A., Connolly, J.A.D., 2008. Constraining the composition and thermal state of mars from inversion of geophysical data. J. Geophys. Res. (Planets) 113, 7003. http://dx.doi.org/10.1029/2007JE002996.

Khan, A., Connolly, J.A.D., Pommier, A., Noir, J., 2014. Geophysical evidence for melt in the deep lunar interior and implications for lunar evolution. J. Geophys. Res. (Planets) 119, 2197–2221. http://dx.doi.org/10.1002/2014JE004661.

Khan, A., Huang, D., Durán, C., Sossi, P.A., Giardini, D., Murakami, M., 2023. Evidence for a liquid silicate layer atop the martian core. Nature 622 (7984), 718–723. http://dx.doi.org/10.1038/s41586-023-06586-4.

Khan, A., Liebske, C., Rozel, A., Rivoldini, A., Nimmo, F., Connolly, J.A.D., Plesa, A.-C., Giardini, D., 2018. A geophysical perspective on the bulk composition of mars. J. Geophys. Res.: Planets 2017JE005371. http://dx.doi.org/10.1002/2017JE005371.

Khan, A., Sossi, P.A., Liebske, C., Rivoldini, A., Giardini, D., 2022. Geophysical and cosmochemical evidence for a volatile-rich mars. Earth Planet. Sci. Lett. 578, 117330. http://dx.doi.org/10.1016/j.epsl.2021.117330.

Kim, D., Banerdt, W.B., Ceylan, S., Giardini, D., Lekić, V., Lognonné, P., Beghein, C., Beucler, É., Carrasco, S., Charalambous, C., Clinton, J., Drilleau, M., Durán, C., Golombek, M., Joshi, R., Khan, A., Knapmeyer-Endrun, B., Li, J., Maguire, R., Pike, W.T., Samuel, H., Schimmel, M., Schmerr, N.C., Stähler, S.C., Stutzmann, E., Wieczorek, M., Xu, Z., Batov, A., Bozdag, E., Dahmen, N., Davis, P., Gudkova, T., Horleston, A., Huang, Q., Kawamura, T., King, S.D., McLennan, S.M., Nimmo, F., Plasman, M., Plesa, A.C., Stepanova, I.E., Weidner, E., Zenhäusern, G., Daubar, I.J., Fernando, B., Garcia, R.F., Posiolova, L.V., Panning, M.P., 2022. Surface waves and crustal structure on mars. Science 378 (6618), 417–421. http://dx.doi.org/10.1126/science.abq7157.

Kim, D., Durán, C., Giardini, D., Plesa, A.-C., Stähler, S.C., Boehm, C., Lekić, V., McLennan, S.M., Ceylan, S., Clinton, J.F., Davis, P., Khan, A., Knapmeyer-Endrun, B., Panning, M.P., Wieczorek, M., Lognonné, P., Banerdt, W.B., 2023. Global crustal thickness revealed by surface waves orbiting mars. Geophys. Res. Lett. 50 (12), e2023GL103482. http://dx.doi.org/10.1029/2023GL103482, e2023GL103482 2023GL103482.

Kleine, T., Nimmo, F., 2024. In: Anbar, A.D., Weis, D. (Eds.), Origin of the Earth. Vol. 5, Elsevier, pp. 1–57.

Konopliv, A.S., Park, R.S., Rivoldini, A., Baland, R.-M., Le Maistre, S., Van Hoolst, T., Yseboodt, M., Dehant, V., 2020. Detection of the chandler wobble of mars from orbiting spacecraft. Geophys. Res. Lett. 47 (21), e90568. http://dx.doi.org/10.1029/2020GL090568.

Kruijer, T.S., Kleine, T., Borg, L.E., 2020. The great isotopic dichotomy of the early solar system. Nat. Astron. 4 (1), 32–40.

Lambrechts, M., Johansen, A., 2012. Rapid growth of gas-giant cores by pebble accretion. Astron. Astrophys. 544, A32. http://dx.doi.org/10.1051/0004-6361/201219127.

Le Maistre, S., Rivoldini, A., Caldiero, A., Yseboodt, M., Baland, R.-M., Beuthe, M., Van Hoolst, T., Dehant, V., Folkner, W.M., Buccino, D., Kahan, D., Marty, J.-C., Antonangeli, D., Badro, J., Drilleau, M., Konopliv, A., Péters, M.-J., Plesa, A.-C., Samuel, H., Tosi, N., Wieczorek, M., Lognonné, P., Panning, M., Smrekar, S., Banerdt, W.B., 2023. Spin state and deep interior structure of mars from InSight radio tracking. Nature 619 (7971), 733–737. http://dx.doi.org/10.1038/s41586-023-06150-0.

Levison, H.F., Kretke, K.A., Walsh, K.J., Bottke, W.F., 2015. Growing the terrestrial planets from the gradual accumulation of sub-meter sized objects. Proc. Natl. Acad. Sci. 112 (4), 14180–14185. http://dx.doi.org/10.1073/pnas.1513364112.

Liebske, C., Khan, A., 2019. On the principal building blocks of mars and earth. Icarus 322, 121–134.

Lodders, K., 2023. Relative atomic solar system abundances, mass fractions, and atomic masses of the elements and their isotopes, composition of the solar photosphere, and compositions of the major chondritic meteorite groups. Space Sci. Rev. 217 (3), 44.

Lodders, K., Fegley, B., 1997. An oxygen isotope model for the composition of mars. Icarus 126 (2), 373–394. http://dx.doi.org/10.1006/icar.1996.5653.

Lognonné, P., Banerdt, W.B., Clinton, J., Garcia, R.F., Giardini, D., Knapmeyer-Endrun, B., Panning, M., Pike, W.T., 2023. Mars seismology. Annu. Rev. Earth Planet. Sci. 51, 643–670. http://dx.doi.org/10.1146/annurev-earth-031621-073318.

Longhi, J., Knittle, E., Holloway, J.R., Wänke, H., 1992. The bulk composition, mineralogy and internal structure of mars. In: Kieffer, H.H., Jakosky, B.M., Snyder, C.W., Matthews, M.S. (Eds.), Mars. Univ of Arizona Press, pp. 184–208.

Lyons, J., Young, E., 2005. CO self-shielding as the origin of oxygen isotope anomalies in the early solar nebula. Nature 435 (7040), 317–320.

Mah, J., Brasser, R., Bouvier, A., Mojzsis, S.J., 2022. Effects of pebble accretion on the growth and composition of planetesimals in the inner solar system. Mon. Not. R. Astron. Soc. 511 (1), 158–175. http://dx.doi.org/10.1093/mnras/stab3766.

McGetchin, T.R., Smyth, J.R., 1978. The mantle of mars: Some possible geological implications of its high density. Icarus 34 (3), 512–536. http://dx.doi.org/10.1016/0019-1035(78)90042-8.

McLennan, S.M., Grotzinger, J.P., Hurowitz, J.A., Tosca, N.J., 2019. The sedimentary cycle on early mars. Annu. Rev. Earth Planet. Sci. 47, 91–118. http://dx.doi.org/10.1146/annurev-earth-053018-060332.

McSween, H.Y., Stolper, E., 1980. Basaltic meteorites. Sci. Am. 242, 54–63. http://dx.doi.org/10.1038/scientificamerican0680-54.

McSween, H.Y., Stolper, E.M., Taylor, L.A., Muntean, R.A., O'Kelley, G.D., Eldridge, J.S., Biswas, S., Ngo, H.T., Lipschutz, M.E., 1979. Petrogenetic relationship between allan hills 77005 and other achondrites. Earth Planet. Sci. Lett. 45 (2), 275–284. http://dx.doi.org/10.1016/0012-821X(79)90129-8.

McSween, Jr., H.Y., 2015. Petrology on mars. Am. Mineral. 100 (11–12), 2380–2395. http://dx.doi.org/10.2138/am-2015-5257.

Mezger, K., Schönbächler, M., Bouvier, A., 2020. Accretion of the earth—missing components? Space Sci. Rev. 216 (2), 27. http://dx.doi.org/10.1007/s11214-020-00649-y.

Mocquet, A., Vacher, P., Grasset, O., Sotin, C., 1996. Theoretical seismic models of mars: the importance of the iron content of the mantle. Planets Space Sci. 44, 1251–1268. http://dx.doi.org/10.1016/S0032-0633(96)00086-4.

Mohapatra, R.K., Murty, S.V.S., 2003. Precursors of mars–constraints from nitrogen and oxygen isotopic compositions of martian meteorites. Meteorit. Planet. Sci. 38, 225–242. http://dx.doi.org/10.1111/j.1945-5100.2003.tb00261.x.

Morbidelli, A., Kleine, T., Nimmo, F., 2025. Did the terrestrial planets of the solar system form by pebble accretion? Earth Planet. Sci. Lett. 650, 119120. http://dx.doi.org/10.1016/j.epsl.2024.119120.

Mosegaard, K., Tarantola, A., 1995. Monte Carlo sampling of solutions to inverse problems. J. Geophys. Res.: Solid Earth (1978– 2012) 100 (B7), 12431–12447.

Moynier, F., Day, J.M., Okui, W., Yokoyama, T., Bouvier, A., Walker, R.J., Podosek, F.A., 2012. Planetary-scale strontium isotopic heterogeneity and the age of volatile depletion of early solar system materials. Astrophys. J. 758 (1), 45.

Palme, H., O'Neill, H.S.C., 2003. Cosmochemical estimates of mantle composition. Treatise Geochem. 2, 568. http://dx.doi.org/10.1016/B0-08-043751-6/02177-0.

Posiolova, L.V., Lognonné, P., Banerdt, W.B., Clinton, J., Collins, G.S., Kawamura, T., Ceylan, S., Daubar, I.J., Fernando, B., Froment, M., Giardini, D., Malin, M.C., Miljkovic, K., Stähler, S.C., Xu, Z., Banks, M.E., Beucler, E., Cantor, B.A., Charalambous, C., Dahmen, N., Davis, P., Drilleau, M., Dundas, C.M., Durán, C., Euchner, F., Garcia, R.F., Golombek, M., Horleston, A., Keegan, C., Khan, A., Kim, D., Larmat, C., Lorenz, R., Margerin, L., Menina, S., Panning, M., Pardo, C., Perrin, C., Pike, W.T., Plasman, M., Rajšić, A., Rolland, L., Rougier, E., Speth, G., Spiga, A., Stott, A., Susko, D., Teanby, N.A., Valeh, A., Werynski, A., Wójcicka, N., Zenhäusern, G., 2022. Largest recent impact craters on mars: Orbital imaging and surface seismic co-investigation. Science 378 (6618), 412–417. http://dx.doi.org/10.1126/science.abq7704.

Rani, A., Basu Sarbadhikari, A., Hood, D., Gasnault, O., Nambiar, S., Karunatillake, S., 2022. Consolidated chemical provinces on mars: Implications for geologic interpretations. Geophys. Res. Lett. 49 (14), e2022GL099235.

Render, J., Brennecka, G.A., Burkhardt, C., Kleine, T., 2022. Solar system evolution and terrestrial planet accretion determined by Zr isotopic signatures of meteorites. Earth Planet. Sci. Lett. 595, 117748.

Righter, K., Drake, M.J., Scott, E.R.D., 2006. Compositional relationships between meteorites and terrestrial planets. In: Lauretta, D.S., McSween, H.Y. (Eds.), Meteorites and the Early Solar System II. pp. 803–828.

Ringwood, A.E., 1966. Chemical evolution of the terrestrial planets. Geochim. Cosmochim. Acta 30 (1), 41–104.

Rivoldini, A., Van Hoolst, T., Verhoeven, O., Mocquet, A., Dehant, V., 2011. Geodesy constraints on the interior structure and composition of mars. Icarus 213, 451–472. http://dx.doi.org/10.1016/j.icarus.2011.03.024.

Rubie, D., Jacobson, S., Morbidelli, A., O'Brien, D., Young, E., de Vries, J., Nimmo, F., Palme, H., Frost, D., 2015. Accretion and differentiation of the terrestrial planets with implications for the compositions of early-formed solar system bodies and accretion of water. Icarus 248, 89–108. http://dx.doi.org/10.1016/j.icarus.2014.10.015.

Rüfenacht, M., Morino, P., Lai, Y.-J., Fehr, M.A., Haba, M.K., Schönbächler, M., 2023. Genetic relationships of solar system bodies based on their nucleosynthetic Ti isotope compositions and sub-structures of the solar protoplanetary disk. Geochim. Cosmochim. Acta 355, 110–125.

Samuel, H., Drilleau, M., Rivoldini, A., Xu, Z., Huang, Q., Garcia, R.F., Lekić, V., Irving, J.C.E., Badro, J., Lognonné, P.H., Connolly, J.A.D., Kawamura, T., Gudkova, T., Banerdt, W.B., 2023. Geophysical evidence for an enriched molten silicate layer above mars's core. Nature 622 (7984), 712–717. http://dx.doi.org/10.1038/s41586-023-06601-8.

Sanloup, C., Jambon, A., Gillet, P., 1999. A simple chondritic model of mars. Phys. the Earth Planet. Inter. 112 (1-2), 43–54. http://dx.doi.org/10.1016/S0031-9201(98)00175-7.

Saxe, J.G., 1873. The Poems of John Godfrey Saxe. James R. Osgood and Co., Boston, Reprinted by University Press: Welch, Bigelow and Co., Cambridge, Massachusetts.

Schiller, M., Bizzarro, M., Fernandes, V.A., 2018. Isotopic evolution of the protoplanetary disk and the building blocks of earth and the moon. Nature 555 (7697), 507–510.

Smrekar, S.E., Lognonné, P., Spohn, T., Banerdt, W.B., Breuer, D., Christensen, U., Dehant, V., Drilleau, M., Folkner, W., Fuji, N., et al., 2019. Pre-mission InSights on the interior of mars. Space Sci. Rev. 215 (1), 3.

Sohl, F., Schubert, G., Spohn, T., 2005. Geophysical constraints on the composition and structure of the martian interior. J. Geophys. Res. (Planets) 110 (E9), 12008. http://dx.doi.org/10.1029/2005JE002520.

Sossi, P.A., Klemme, S., O'Neill, H.S.C., Berndt, J., Moynier, F., 2019. Evaporation of moderately volatile elements from silicate melts: experiments and theory. Geochim. Cosmochim. Acta 260, 204–231.

Sossi, P.A., Stotz, I.L., Jacobson, S.A., Morbidelli, A., O'Neill, H.S.C., 2022. Stochastic accretion of the earth. Nat. Astron. 6 (8), 951–960.

Stähler, S.C., Khan, A., Banerdt, W.B., Lognonné, P., Giardini, D., Ceylan, S., Drilleau, M., Duran, A.C., Garcia, R.F., Huang, Q., Kim, D., Lekic, V., Samuel, H., Schimmel, M., Schmerr, N., Sollberger, D., Stutzmann, É., Xu, Z., Antonangeli, D., Charalambous, C., Davis, P.M., Irving, J.C.E., Kawamura, T., Knapmeyer, M., Maguire, R., Marusiak, A.G., Panning, M.P., Perrin, C., Plesa, A.-C., Rivoldini, A., Schmelzbach, C., Zenhäusern, G., Beucler, É., Clinton, J., Dahmen, N., van Driel, M., Gudkova, T., Horleston, A., Pike, W.T., Plasman, M., Smrekar, S.E., 2021. Seismic detection of the martian core. Science 373 (6553), 443–448. http://dx.doi.org/10.1126/science.abi7730.

Stähler, S.C., Mittelholz, A., Perrin, C., Kawamura, T., Kim, D., Knapmeyer, M., Zenhäusern, G., Clinton, J., Giardini, D., Lognonné, P., et al., 2022. Tectonics of cerberus fossae unveiled by marsquakes. Nat. Astron. 1–11. http://dx.doi.org/10.1038/s41550-022-01803-y.

Steenstra, E.S., van Westrenen, W., 2018. A synthesis of geochemical constraints on the inventory of light elements in the core of mars. Icarus 315, 69–78.

Stixrude, L., Lithgow-Bertelloni, C., 2005. Mineralogy and elasticity of the oceanic upper mantle: Origin of the low-velocity zone. J. Geophys. Res.: Solid Earth 110 (B3), http://dx.doi.org/10.1029/2004JB002965, B03204.

Stixrude, L., Lithgow-Bertelloni, C., 2011. Thermodynamics of mantle minerals - II. Phase equilibria. Geophys. J. Int. 184, 1180–1213. http://dx.doi.org/10.1111/j.1365-246X.2010.04890.x.

Stolper, E., McSween, Jr., H.Y., 1979. Petrology and origin of the shergottite meteorites. Geochim. Cosmochim. Acta 43, 1475–1477. http://dx.doi.org/10.1016/0016-7037(79)90142-X.

Tang, H., Dauphas, N., 2014. Fe-60-Ni-60 chronology of core formation in mars. Earth Planet. Sci. Lett. 390, 264–274. http://dx.doi.org/10.1016/j.epsl.2014.01.005.

Taylor, S.R., 2001. Solar System Evolution: A New Perspective. Cambridge University Press, p. 484.

Taylor, G.J., 2013. The bulk composition of mars. Chem. Erde/Geochem. 73, 401–420. http://dx.doi.org/10.1016/j.chemer.2013.09.006.

Taylor, S.R., McLennan, S., 2009. In: Day, J.M.D. (Ed.), Planetary Crusts: Their Composition, Origin and Evolution. Blackwell Publishing Ltd.

Taylor, G., Stopar, J., Boynton, W., Karunatillake, S., Keller, J., Brückner, J., Wänke, H., Dreibus, G., Kerry, K., Reedy, R., Evans, L., Starr, R., Martel, L., Squyres, S., Gasnault, O., Maurice, S., d'Uston, C., Englert, P., Dohm, J., Baker, V., Hamara, D., Janes, D., Sprague, A., Kim, K., Drake, D., McLennan, S., Hahn, B., 2006. Variations in K/Th on mars. J. Geophys. Res. E: Planets 111 (E3), http://dx.doi.org/10.1029/2006JE002676.

Tian, Z., Magna, T., Day, J.M.D., Mezger, K., Scherer, E.E., Lodders, K., Hin, R.C., Koefoed, P., Bloom, H., Wang, K., 2021. Potassium isotope composition of mars reveals a mechanism of planetary volatile retention. Proc. Natl. Acad. Sci. 118 (39), e2101155118. http://dx.doi.org/10.1073/pnas.2101155118.

Tiesinga, E., Mohr, P., Newell, D., Taylor, B., 2021. CODATA recommended values of the fundamental physical constants: 2018. http://dx.doi.org/10.1103/RevModPhys.93.025010.

Tissot, F.L., Collinet, M., Namur, O., Grove, T.L., 2022. The case for the angrite parent body as the archetypal first-generation planetesimal: Large, reduced and Mg-enriched. Geochim. Cosmochim. Acta 338, 278–301.

Torrano, Z.A., Schrader, D.L., Davidson, J., Greenwood, R.C., Dunlap, D.R., Wadhwa, M., 2021. The relationship between CM and CO chondrites: Insights from combined analyses of titanium, chromium, and oxygen isotopes in CM, CO, and ungrouped chondrites. Geochim. Cosmochim. Acta 301, 70–90.

Trinquier, A., Birck, J.-L., Allegre, C.J., 2007. Widespread Cr-54 heterogeneity in the inner solar system. Astrophys. J. 655 (2, 1), 1179–1185. http://dx.doi.org/10.1086/510360.

Turekian, K.K., Clark, Jr., S.P., 1969. Inhomogeneous accumulation of the earth from the primitive solar nebula. Earth Planet. Sci. Lett. 6 (5), 346–348.

Udry, A., Howarth, G.H., Herd, C.D.K., Day, J.M.D., Lapen, T.J., Filiberto, J., 2020. What martian meteorites reveal about the interior and surface of mars. J. Geophys. Res. (Planets) 125 (12), e06523. http://dx.doi.org/10.1029/2020JE00652310.1002/essoar.10503123.4.

Verhoeven, O., Rivoldini, A., Vacher, P., Mocquet, A., Choblet, G., Menvielle, M., Dehant, V., Van Hoolst, T., Sleewaegen, J., Barriot, J.-P., Lognonné, P., 2005. Interior structure of terrestrial planets: Modeling mars' mantle and its electromagnetic, geodetic, and seismic properties. J. Geophys. Res. (Planets) 110, 4009. http://dx.doi.org/10.1029/2004JE002271.

Walker, D., Stolper, E.M., Hays, J.F., 1979. Basaltic volcanism: the importance of planet size.. Lunar Planet. Sci. Conf. Proc. 2, 1995–2015.

Wang, Y., Wen, L., Weidner, D.J., 2013. Composition of mars constrained using geophysical observations and mineral physics modeling. Phys. Earth Planet. Inter. 224, 68–76. http://dx.doi.org/10.1016/j.pepi.2013.08.005.

Wänke, H., 1981. Constitution of terrestrial planets. Philos. Trans. R. Soc. Lond. Ser. A 303 (1477), 287–301. http://dx.doi.org/10.1098/rsta.1981.0203.

Wänke, H., Dreibus, G., 1988. Chemical composition and accretion history of terrestrial planets. Philos. Trans. R. Soc. Lond. Ser. A 325 (1587), 545–557. http://dx.doi.org/10.1098/rsta.1988.0067.

Wänke, H., Dreibus, G., 1994. Chemistry and accretion history of mars. Philos. Trans. R. Soc. Lond. Ser. A 349, 285–293. http://dx.doi.org/10.1098/rsta.1994.0132.

Warren, P.H., 2011. Stable-isotopic anomalies and the accretionary assemblage of the earth and mars: A subordinate role for carbonaceous chondrites. Earth Planet. Sci. Lett. 311 (1), 93–100. http://dx.doi.org/10.1016/j.epsl.2011.08.047.

Wasson, J.T., Kallemeyn, G.W., 1988. Compositions of chondrites. Philos. Trans. R. Soc. Lond. Ser. A 325, 535–544. http://dx.doi.org/10.1098/rsta.1988.0066.

Wasson, J.T., Wetherill, G.W., 1979. Dynamical chemical and isotopic evidence regarding the formation locations of asteroids and meteorites. In: Gehrels, T., Matthews, M.S. (Eds.), Asteroids. pp. 926–974.

Wetherill, G.W., 1980. Formation of the Terrestrial Planets. Vol. 18, pp. 77–113. http://dx.doi.org/10.1146/annurev.aa.18.090180.000453.

Weyrauch, M., Horstmann, M., Bischoff, A., 2018. Chemical variations of sulfides and metal in enstatite chondrites—Introduction of a new classification scheme. Meteorit. Planet. Sci. 53 (3), 394–415.

Williams, N.H., Fehr, M.A., Parkinson, I.J., Mandl, M.B., Schönbächler, M., 2021. Titanium isotope fractionation in solar system materials. Chem. Geol. 568, 120009.

Witt-Eickschen, G., Palme, H., O'neill, H.S.C., Allen, C.M., 2009. The geochemistry of the volatile trace elements As, Cd, Ga, In and Sn in the earth's mantle: New evidence from in situ analyses of mantle xenoliths. Geochim. Cosmochim. Acta 73 (6), 1755–1778.

Yin, Q., 2005. From dust to planets: The tale told by moderately volatile elements. In: Krot, A.N., Scott, E.R.D., Reipurth, B. (Eds.), Chondrites and the Protoplanetary Disk. In: Astronomical Society of the Pacific Conference Series, vol. 341, p. 632.

Yokoyama, T., Nagai, Y., Fukai, R., Hirata, T., 2019. Origin and evolution of distinct molybdenum isotopic variabilities within carbonaceous and noncarbonaceous reservoirs. Astrophys. J. 883 (1), 62.

Yoshizaki, T., McDonough, W.F., 2020. The composition of mars. Geochim. Cosmochim. Acta 273, 137–162. http://dx.doi.org/10.1016/j.gca.2020.01.011.

Zhang, J., Dauphas, N., Davis, A.M., Leya, I., Fedkin, A., 2012. The proto-earth as a significant source of lunar material. Nat. Geosci. 5 (4), 251–255.

Zharkov, V.N., Gudkova, T.V., 2005. Construction of martian interior model. Sol. Syst. Res. 39, 343–373. http://dx.doi.org/10.1007/s11208-005-0049-7.

Zheng, Y., Nimmo, F., Lay, T., 2015. Seismological implications of a lithospheric low seismic velocity zone in mars. Phys. Earth Planet. Inter. 240, 132–141. http://dx.doi.org/10.1016/j.pepi.2014.10.004.

Zhu, K., Schiller, M., Pan, L., Saji, N.S., Larsen, K.K., Amsellem, E., Rundhaug, C., Sossi, P., Leya, I., Moynier, F., et al., 2022. Late delivery of exotic chromium to the crust of mars by water-rich carbonaceous asteroids. Sci. Adv. 8 (46), eabp8415.